

A comparison between short GRB afterglows and kilonova AT2017gfo: shedding light on kilonovae properties

A. Rossi ^{1,2*}, G. Stratta ^{1,3}, E. Maiorano ¹, D. Spighi, ¹ N. Masetti, ^{1,4} E. Palazzi, ¹ A. Gardini, ⁵ A. Melandri ⁶, L. Nicastro, ¹ E. Pian ¹, M. Branchesi, ⁷ M. Dadina, ¹ V. Testa ², E. Brocato, ^{2,8} S. Benetti, ⁹ R. Ciolfi, ^{9,10} S. Covino ⁶, V. D’Elia, ^{2,11} A. Grado, ¹² L. Izzo ⁵, A. Perego, ¹³ S. Piranomonte, ² R. Salvaterra, ¹⁴ J. Selsing, ¹⁵ L. Tomasella ⁹, S. Yang, ⁹ D. Vergani, ¹ L. Amati ¹ and J. B. Stephen ¹

on behalf of the Gravitational Wave Inaf TeAm (GRAWITA)

¹INAF – Osservatorio di Astrofisica e Scienza dello Spazio, via Piero Gobetti 93/3, I-40129 Bologna, Italy

²INAF – Osservatorio Astronomico di Roma, via Frascati 33, I-00040 Monte Porzio Catone, Italy

³INFN – Firenze, via Sansone 1, I-50019 Firenze, Italy

⁴Departamento de Ciencias Físicas, Universidad Andrés Bello, Av. Fernández Concha 700, 7591538 Las Condes, Santiago, Chile

⁵Instituto de Astrofísica de Andalucía (IAA-CSIC), Glorieta de la Astronomía s/n, E-18008 Granada, Spain

⁶INAF – Osservatorio Astronomico di Brera, Via E. Bianchi 46, I-23807 Merate (LC), Italy

⁷Gran Sasso Science Institute, Viale F. Crispi 7, I-67100 L’Aquila, Italy

⁸INAF – Osservatorio Astronomico d’Abruzzo, Via M. Maggini snc, I-64100 Teramo, Italy

⁹INAF – Osservatorio Astronomico di Padova, Vicolo dell’Osservatorio 5, I-35122 Padova, Italy

¹⁰INFN – Sezione di Padova, Via Francesco Marzolo 8, I-35131 Padova, via Sommarive 14, I-38123 Trento, Italy

¹¹ASI-Science Data Center, via del Politecnico snc, I-00133 Rome, Italy

¹²INAF – Osservatorio Astronomico di Capodimonte, salita Moiariello 16, I-80131 Napoli, Italy

¹³Università degli Studi di Milano-Bicocca, Piazza dell’Ateneo Nuovo, 1, I-20126, Milano, Italy

¹⁴INAF – Istituto di Astrofisica Spaziale e Fisica Cosmica di Milano, via E. Bassini 15, I-20133 Milano, Italy

¹⁵Dark Cosmology Centre, Niels Bohr Institute, Juliane Maries Vej 30, DK-2100 Copenhagen Ø, Denmark

Accepted 2020 February 4. Received 2020 January 9; in original form 2019 January 8

ABSTRACT

Multimessenger astronomy received a great boost following the discovery of kilonova (KN) AT2017gfo, the optical counterpart of the gravitational wave source GW170817 associated with the short gamma-ray burst GRB 170817A. AT2017gfo was the first KN that could be extensively monitored in time using both photometry and spectroscopy. Previously, only few candidates have been observed against the glare of short GRB afterglows. In this work, we aim to search the fingerprints of AT2017gfo-like KN emissions in the optical/NIR light curves of 39 short GRBs with known redshift. For the first time, our results allow us to study separately the range of luminosity of the blue and red components of AT2017gfo-like kilonovae in short GRBs. In particular, the red component is similar in luminosity to AT2017gfo, while the blue KN can be more than 10 times brighter. Finally, we exclude a KN as luminous as AT2017gfo in GRBs 050509B and 061201.

Key words: gravitational waves – gamma-ray burst: general – gamma-ray bursts – neutron star mergers – stars: magnetars.

1 INTRODUCTION

Gamma-ray bursts (GRBs) are divided in two populations consisting of long and short GRBs (e.g. Kouveliotou et al. 1993). Long GRBs (i.e. GRBs with a burst duration longer than ~ 2 s) have been

conclusively linked to the explosive deaths of massive stars (e.g. Hjorth et al. 2003). For a long time, only indirect evidence associated short GRBs to the merging of compact objects, however a watershed occurred after the simultaneous detection of the gravitational wave (GW) source GW170817 (Abbott et al. 2017a) by aLIGO/AdVirgo (Acernese et al. 2015; LIGO Scientific Collaboration 2015) and the short GRB 170817A (Abbott et al. 2017c; Goldstein et al. 2017; Savchenko et al. 2017). Their identification with the same

* E-mail: andrea.rossi@inaf.it

astrophysical source has provided the first direct evidence that at least a fraction of short GRBs is associated with the merging of two neutron stars (NSs). At the same time, the discovery of the optical counterpart of GW170817, AT2017gfo (Coulter et al. 2017), and its identification with the elusive ‘kilonova’ (KN) emission (e.g. Li & Paczyński 1998; Metzger et al. 2010), has indirectly told us that these poorly sampled astrophysical phenomena can potentially be detected as a possible additional component to the optical and near-infrared (NIR) afterglow of (nearby) short GRBs in the temporal window that goes from about a few hours to a few weeks after the onset of the burst (e.g. Kasen, Fernández & Metzger 2015; Barnes et al. 2016; Fernández & Metzger 2016; Metzger 2017).

AT2017gfo was discovered during its brightening phase at ~ 11 h after the GW event (Coulter et al. 2017) and was followed up by several groups both photometrically and spectroscopically in the optical and NIR bands (Andreoni et al. 2017; Arcavi et al. 2017; Chornock et al. 2017; Covino et al. 2017; Drout et al. 2017; Evans et al. 2017; Kasliwal et al. 2017a; Pian et al. 2017; Smartt et al. 2017; Tanvir et al. 2017; Troja et al. 2017). This enormous observational effort, well summarized in Abbott et al. (2017b), allowed several of these groups to recognize a thermal emission in the data, with a blackbody temperature evolving from ~ 7300 K at ~ 0.6 d (Evans et al. 2017) to ~ 5000 K at 1.5 d after the GW event (Pian et al. 2017; Smartt et al. 2017). At ~ 6 d, the maximum moved to the longer wavelengths peaking in the *J* band, indicating rapid cooling. This behaviour was markedly different not only from an afterglow but also from a supernova event. Instead, both the light-curve evolution and the early (< 15 d) spectra nicely matched the expected KN modelling, i.e. a thermal emission powered by the radioactive decay of elements formed via r-process nucleosynthesis in the ejecta of the NS–NS merger (e.g. Kasen et al. 2017; Metzger, Thompson & Quataert 2018). In particular, the observations are consistent with a KN characterized by a blue, rapidly decaying, component and a red, more slowly evolving, component. Moreover, Covino et al. (2017) reported a low degree of linear polarization of the optical blue component which is consistent with a symmetric geometry of the emitting region and with low inclination of the merger system.

At the same position of AT2017gfo, a non-thermal emission consistent with a GRB afterglow was first identified in the X-ray and radio bands no more than one week after the GW event (Hallinan et al. 2017; Troja et al. 2017), and only months later in the optical (Lyman et al. 2018; Margutti et al. 2018; Rossi et al. 2018b; Piro et al. 2019) due to Sun observational constraints. Afterwards, the multiwavelength follow-up continued for up to one year after the GW event (D’Avanzo et al. 2018; Troja et al. 2018b; Piro et al. 2019). The observations show an achromatic slow rising flux up to ~ 150 d after the explosion followed by a decay and are interpreted as emission from a structured jet expanding in the ISM and observed off-axis from a viewing angle of ~ 20 deg with respect to the jet axis (Kathirgamaraju, Barniol Duran & Giannios 2018; Mooley et al. 2018a; Troja et al. 2018b; Ghirlanda et al. 2019; Kathirgamaraju et al. 2019; Salafia et al. 2019). This is consistent with the inclination of the system derived combining the GW signal and the distance of the source (Abbott et al. 2017c; Mandel 2018). Such a scenario predicts a late-time rising afterglow, in contrast with the on-axis case (i.e. when the viewing angle is along, or very close to, the jet axis). The afterglow observations and their consistency with the off-axis model further confirm that all the early (i.e. < 1 month after the GW event) optical/NIR data of AT2017gfo are not contaminated by the afterglow emission, as the latter is initially much fainter as it was already noticed (e.g. Pian et al. 2017).

The precise nature of the different ejection mechanisms and of the different ejecta components is still under debate (Kasen

et al. 2017; Perego, Radice & Bernuzzi 2017; Metzger et al. 2018; Radice et al. 2018; Tanaka et al. 2018). Numerical simulations show that, during the merger of two NSs, a small fraction ($\sim 0.05 M_{\odot}$ or less) of the total mass is ejected into space with a latitude-dependent pattern of density, velocity, and opacity. Specifically, it is thought that along the polar regions the ejecta have lower velocities and opacities (the *blue* KN component; Kasen et al. 2017) with respect to the equatorial region if an NS remnant is formed after the merger. If a black hole (BH) is promptly formed, the ejecta are mostly concentrated on the equatorial plane and have high velocity and large opacities (the *red* KN component; Kasen et al. 2017). The analysis of the complete set of data of AT2017gfo has clearly demonstrated that early ultraviolet (UV) and optical observations are of key importance to disentangle the different thermal contributions that are present in the observed emission (e.g. Cowperthwaite et al. 2017; Pian et al. 2017; Villar et al. 2017; Arcavi 2018; Bulla et al. 2019) and at least two, possibly three, different emitting components have been identified (e.g. Perego et al. 2017).

The most plausible evidence of a KN before AT2017gfo is that observed as an emerging component in the light curve of the NIR afterglow of the short GRB 130603B at $z = 0.356$ (Berger, Fong & Chornock 2013b; Tanvir et al. 2013). Other possible KN signatures were found in the optical counterpart light curves of GRBs 050709 at $z = 0.161$ (Jin et al. 2016), 060614 at $z = 0.125$ (Jin et al. 2015; Yang et al. 2015), 080503 (Perley et al. 2009; Gao et al. 2017) at unknown redshift, 150101B at $z = 0.134$ (Troja et al. 2018b), and both in the NIR and (perhaps less clearly) in the optical counterpart light curve of 160821B at $z = 0.16$ (Kasliwal et al. 2017b; Jin et al. 2018; Lamb et al. 2019; Troja et al. 2019). Gao et al. (2017) found three other possible KN candidates associated with GRBs 050724, 070714B, and 061006. However, their peak luminosity at ~ 1 d after the burst are more than one order of magnitude brighter than the typical predicted values of the KN associated with GRBs 050709 and 130603B. It should also be noted that in all these possible KN identifications (but GRB 150101B), the emission was preceded by a bright GRB afterglow indicating an on-axis configuration, thus suggesting that the KN emission may exceed the afterglow luminosity even for on-axis GRBs.

After the discovery of AT2017gfo, Gompertz et al. (2018) compared the optical/NIR light curves of AT2017gfo with those of 23 short GRBs with redshift below 0.5. They were able to firmly exclude the presence of an AT2017gfo-like component in three GRBs (050509B, 061201, and 080905A). At the same time, they confirmed that AT2017gfo was much fainter than the claimed KN candidates (see also Fong et al. 2017). These results suggest that kilonovae may display very different luminosity, colours, and time-scale evolutions.

To further investigate the possible range of KN luminosity, we compare the optical/NIR light curves of all short GRB with known redshift up to 2019 June with those of AT2017gfo. This paper is organized as follows. In Section 2, we describe the AT2017gfo data used in this work and the short GRB sample selection. In Section 3, we describe the methods we used to compare AT2017gfo with other short GRB optical/NIR counterparts. Section 4 then illustrates the results about the most compelling short GRBs. These results are then discussed in Section 5. Finally, our conclusions are given in Section 6.

Throughout this work, we adopt the notation according to which the flux density of a counterpart is described as $F_{\nu}(t) \propto t^{-\alpha} \nu^{-\beta}$ and we use a Λ CDM world model with $\Omega_{\text{M}} = 0.308$, $\Omega_{\Lambda} = 0.692$, and $H_0 = 67.8 \text{ km s}^{-1} \text{ Mpc}^{-1}$ (Planck Collaboration XIII 2016).

2 DATA

In this section, we describe spectroscopic and photometric data of AT2017gfo, and the optical/NIR photometric data of short GRBs with known redshift that we compiled and used in this work.

2.1 AT2017gfo data

The follow-up with VLT/X-Shooter of AT2017gfo is not only the first spectroscopic observation of a KN, but it also provided the first temporal sampling of this new class of sources. The 10 spectra, described in Pian et al. (2017) and Smartt et al. (2017), were taken between ~ 1.5 and ~ 10.5 d after the GW trigger and have a coverage from UV to NIR bands. We did not consider Gemini-S/GMOS and VLT/FORS spectroscopic observations which are limited only to the optical window. All but two epochs are obtained from Pian et al. (2017). The two epochs at ~ 2.5 and ~ 4.5 after the GW trigger are from Smartt et al. (2017)¹ and have been taken from the last version available on *WiSeREP* (Yaron & Gal-Yam 2012).

At epochs earlier than the first spectrum (i.e. < 1.5 d after the GW trigger), we have collected photometric observations from the works of Tanvir et al. (2017), Drout et al. (2017), Evans et al. (2017), Covino et al. (2017), Coulter et al. (2017), Troja et al. (2017), Pian et al. (2017), Cowperthwaite et al. (2017); see also the Kilonova Project: Guillochon et al. (2017). We interpolated the photometric light curves using a cubic spline to build the spectral energy distribution (SEDs) at three epochs. The first epoch at ~ 0.5 d after the trigger roughly corresponds to the first optical/NIR observations, the second epoch at 0.66 d is the first one with UV data, and the third epoch at ~ 1 d after the trigger lays between the first photometric and the first X-Shooter observations (Fig. 1). Note that we did not use all data available in the literature, because these data show great variation in values, even though the single data points have in most cases very small uncertainties. This can be ascribed to different calibration and the problematic removal of light from the underlying host galaxy. Therefore, we decided to use only photometric data from large telescopes and from the restricted number of works given above.

All data have been corrected for the Galactic absorption using the interstellar extinction curve derived by Cardelli, Clayton & Mathis (1989), the dust maps of Schlafly & Finkbeiner (2011), and an optical total-to-selective extinction ratio $R_V = 3.1$. All observations have been converted to flux densities F_ν using transmission curves or instrument-specific conversion factors when available, or the standard conversions following Blanton & Roweis (2007).

2.2 The short GRB data sample

Our starting sample of short GRBs is that presented by Fong et al. (2015) which includes 87 short GRBs with optical and NIR counterparts observed between 2004 November and 2015 March. We considered only the 33 events that have a redshift determination. We extended this sample by including six short GRBs with known redshift, detected between 2015 March and 2019 June.

In addition, we took into account many works that show that the short/hard versus long/soft division does not map directly on to what would be expected from the two classes of progenitors (e.g. Kann et al. 2011). For instance, Bromberg et al. (2012) showed that the 2 s duration commonly used to separate collapsars and non-collapsars is inconsistent with the duration distributions of *Swift* and *Fermi* GRBs

Table 1. The 39 short GRBs used in this work.

GRB	z	$P_{cc}(< \delta R)$ _{<i>a</i>}	References _{<i>b</i>}	Accurate redshift ^c
050509B ^d	0.225	5×10^{-3}	1-2	y
050709 ^d	0.161	3×10^{-3}	1	y
050724 ^d	0.258	2×10^{-5}	1	y
051221A	0.546	5×10^{-5}	1	y
060502B	0.287	0.03	1-3	n
060614 ^e	0.125 ^f	–	1-4	y
060801	1.13	0.02	1-3	n
061006 ^d	0.438	4×10^{-4}	1	y
061201 ^d	0.111	0.08	1-5-6	n
061210 ^d	0.41	0.02	1-3	y
061217	0.827	0.24	1-5	n
070429B	0.902	3×10^{-3}	1	y
070714B ^d	0.923	5×10^{-3}	1	y
070724A ^d	0.456	8×10^{-4}	1	y
070729	0.8	0.05	1-5-7	y
070809	0.473	0.03	1-4-6	n
071227 ^d	0.381	0.01	1	y
080905A ^d	0.122	0.01	1	n
090510 ^d	0.903	8×10^{-3}	1-5	y
090515	0.403	0.15	1-4	n
100117A	0.915	7×10^{-5}	1	y
100206A	0.407	1×10^{-3}	1-8	y
100625A	0.452	0.04	1	y
100816A ^e	0.805 ^f	–	9	y
101219A	0.718	0.06	1	y
111117A	2.211	0.02	1-10-11	y
120804A	1.3	210 – 4	12	y
130603B ^d	0.356 ^f	–	13	y
131004A	0.717 ^f	–	14-15	y
140903A ^d	0.351	3×10^{-4}	16	y
141212A	0.596	0.03	17-18-this work	n
150101B	0.134	4.8×10^{-4}	19	y
150120A	0.46	0.02	20-21-this work	n
150423A ^e	1.394 ^f	See text	22-23	n
150424A ^e	0.3	0.02	24-25-26-this work	n
160410A ^e	1.717 ^f	–	22	y
160624A ^e	0.483	0.01	27-this work	y
160821B ^e	0.16	0.02	28-29	y
170428A ^e	0.454	4×10^{-3}	30-this work	y

^aProbability of chance coincidence (Bloom, Kulkarni & Djorgovski 2002).

^bReferences for the probability of chance association and redshift: (1) Fong et al. (2013); (2) Bloom et al. (2006); (3) Berger et al. (2007); (4) (Price, Berger & Fox 2006); (5) Berger (2010); (6) Stratta et al. (2007); (7) Fong & Berger (2013); (8) Perley et al. (2012); (9) (Tanvir et al. 2010); (10) Margutti et al. (2012); (11) Selsing et al. (2018); (12) Berger et al. (2013a); (13) de Ugarte Postigo et al. (2014); (14) Chornock, Lunnan & Berger (2013); (15) D’Elia et al. (2013); (16) Troja et al. (2016); (17) Malesani et al. (2014); (18) Chornock, Fong & Fox (2014); (19) Fong et al. (2016); (20) Chornock & Fong (2015); (21) Perley & Cenko (2015); (22) (Selsing et al. 2019); (23) (Malesani et al. 2015); (24) (Castro-Tirado et al. 2015); (25) Jin et al. (2018); (26) Tanvir et al. (2015); (27) (Cucchiara & Levan 2016); (28) (Levan et al. 2016); (29) Troja et al. (2019); (30) (Izzo et al. 2017).

^cSee Section 2.3

^dLight curve updated with respect to Fong et al. (2015) with new data. See Table A2.

^eNot in Fong et al. (2015), photometry in Table A2.

^fRedshift measured from the afterglow spectrum. In these cases, association with a host galaxy was not necessary and therefore not reported.

¹They are limited to ~ 22000 Å due to the presence of *K*-band blocking filter.

and only holds for old BATSE GRBs. For this reason, we included the two peculiar long GRBs 060614 and 100816A, because their spectral hardness and negligible spectral lags are typical of short GRBs (see also Bernardini et al. 2015). With respect to the Fong et al. (2015) sample, we removed GRB 140622A because only very early upper limits exist (i.e. <0.1 h after trigger) that could not be compared with AT2017gfo observations that started 0.5 d after the trigger. We also excluded GRB 090426 which, although having a duration shorter than 2 s, has features similar to collapsar events (soft spectra, dwarf blue host, very luminous afterglow, Antonelli et al. 2009; Nicuesa Guelbenzu et al. 2011, 2012). In addition, we have also updated the light curves of the whole short GRB sample by adding photometric measurements that were not included in the original Fong et al. (2015) data set (see Table A2). Finally, we have updated the redshift of GRB 111117A with the more refined measure of $z = 2.211$ (Sakamoto et al. 2013; Selsing et al. 2018). Note that, contrary to Gompertz et al. (2018), we decided to not include GRB 051210 because, according to the most recent literature, only a lower limit on the redshift exists ($z > 1.4$, see Berger et al. 2007; Fong et al. 2015). The final sample thus consists of 39 short GRBs within the redshift range $0.1 \leq z \leq 2.2$ and is summarized in Table 1.

In all cases, we pay particular attention to not include photometry that was dominated by the host according to the literature from which we obtained the data. In the case the origin of the emission was not specified or was not certain in the literature, then we considered only data that showed to be fading. However, in all cases we have not considered necessary to model the light curves to search for a constant component, i.e. the host.

2.3 On the redshift accuracy

Accurate and reliable redshift determination through optical/NIR spectroscopy of short GRB afterglows have been obtained only in three cases (GRBs 100816A, 130603B, 160410A). In case of GRBs 060614 and 131004A, the redshift is measured from emission lines of the host superposed from the afterglow spectrum.² In all other 34 cases, the redshifts have been obtained through spectroscopy of the associated host galaxies. To assess the probability that the burst originated from a host candidate, we have collected or calculated the probability of chance coincidence, $P_{cc}(< \delta R)$ (Bloom et al. 2002), at a given angular separation (δR), and apparent magnitude (m) for galaxies candidates.

In Table 1, we indicate redshifts, probabilities, and their references. In few cases, the probabilities are not negligible (larger than 1 per cent), but given the lack of any other possible galaxy with similarly low chance association, they are considered as good association. They are GRBs 061210, 070729, 100625A, 101219A, 111117A. In nine cases, no clear association can be made with a galaxy in the field (GRBs 060502B, 060801, 061201, 061217, 070809, 090515, 141212A, 150120A, 150424A). Therefore, they do not have well-defined redshift measurements.

In almost all other cases, the association with the host is well defined following the criteria of Bloom et al. (2002) and it was possible to measure a redshift (Table 1). Only two cases deserve more caution: GRBs 080905A and 150423A. In the first case, D’Avanzo et al. (2014) find that its properties are not consistent with the $E_{\text{peak}}-L_{\text{iso}}$ (Yonetoku et al. 2004), and the $E_{\text{peak}}-E_{\text{iso}}$ relations (Amati et al. 2002). They conclude that either GRB 080905A

is really a peculiar subluminal (and subenergetic) burst, or the associated host galaxy is just a foreground source, and the distance is underestimated. In the case of GRB 150423A, we adopted the redshift of $z = 1.394$ measured by Malesani et al. (2014) and Selsing et al. (2019). However, as noted in Malesani et al. (2014) the redshift is based only on a tentative detection of an absorption doublet in the faint afterglow continuum, and identified as Mg II at $z = 1.394$. Our independent analysis of the reduced spectrum has not permitted us to confirm the presence of the absorption lines. We note that Perley (2015) reports the presence of a galaxy at redshift of $z = 0.456$ with $r = 23.3$ (Varela, Knust & Greiner 2015) and $4''$ away from the afterglow position (with $P_{cc} = 0.13$) and thus leaving the distance measurement for this burst still uncertain.

Finally, in the case of GRB 061201 we used the redshift of 0.111 of the nearest galaxy (Stratta et al. 2007), used also by Fong et al. (2015), which is different from $z = 0.084$ used by Gompertz et al. (2018) that is the redshift of the galaxy cluster within which this GRB happened. In summary, we estimate that for 28 short GRBs out of 39 events, the associated redshift is highly reliable.

3 DATA ANALYSIS

In order to compare AT2017gfo with GRB optical counterparts, we computed the AT2017gfo luminosity in the GRB rest-frame filters. This approach allows us to use the exceptionally high-quality data set of AT2017gfo which provides much better spectral accuracy and coverage than that of typical GRB afterglows, enabling a more precise flux estimate in the redshifted frequencies. We thus first built a set of rest-frame AT2017gfo spectra at different epochs, which hereafter we will refer as KN spectral templates. We then convolved these spectra with the optical/NIR filters scaled to the rest frame of each GRB and proceeded with the luminosity comparison.

This procedure is similar to that used by Gompertz et al. (2018). However, the use of X-Shooter spectra allows us to simplify the approach. First of all, except for the blackbody modelling of the photometry for the first three epochs, we do not interpolate the SED to obtain the photometry in a specific filter, because the X-Shooter spectroscopy guarantees full spectral coverage. Secondly, we do not need to make any special assumption for the bluer part of the spectra of AT2017gfo, because the X-Shooter spectra extends down to 3500 Å (including half of the U band). With our method, we can give robust constraints to the rest-frame optical data (<6000 Å) up to redshift ~ 0.7 . We also note that, in our case, we do not use an analytical function to model the light curves, since we have better temporal sampling. Instead, we interpolate the photometry derived from the spectral templates when we need to compute the luminosity ratio (Table A1). Below we explain all the steps of this analysis in more detail.

3.1 Kilonova spectral templates

After including the three SEDs built at 0.5, 0.66, and 1 d after the trigger, we have a total of 13 epochs that we use to build the KN spectral templates.

We modelled the three SEDs following the current theoretical interpretation of AT2017gfo, where the observed emission is the combination of at least two different blackbody components.³

³We note that a more sophisticated model has been used by other authors (Cowperthwaite et al. 2017; Villar et al. 2017) who found some evidence of an intermediate blackbody component. However, given that our goal is only to model the extremes of the spectral interval, we considered that an intermediate component is too sophisticated for the aim of this work.

²In case of GRB 131004A possible weak absorption lines at this same redshift are also present (Chornock et al. 2013).

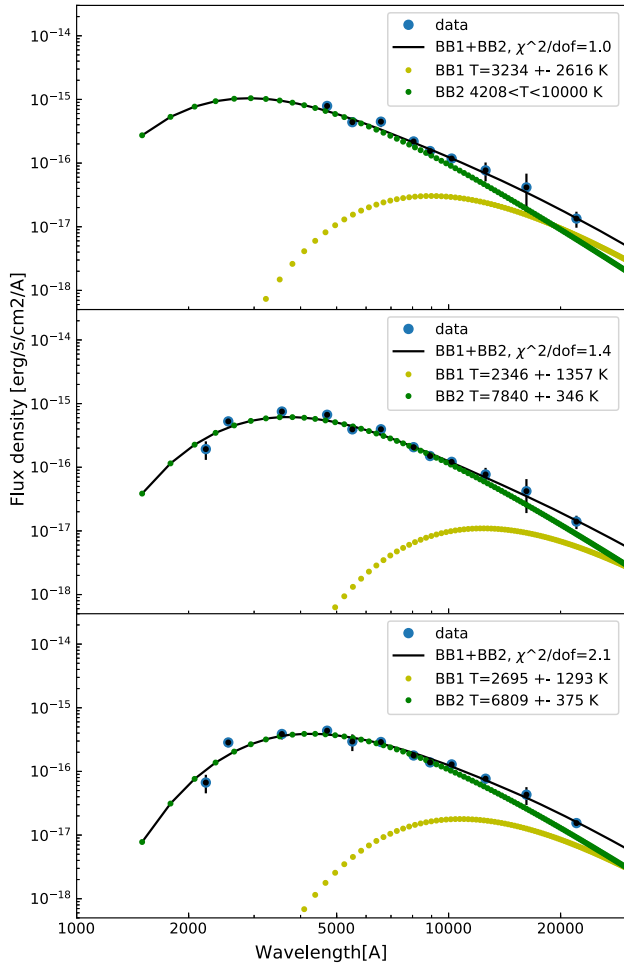


Figure 1. Photometry at 0.5, 0.66, and 1 d after trigger (blue dots with errorbars) of AT2017gfo modelled with a double blackbody model (in black), with single blackbody components in green and yellow (see Section 3.1).

Results are plotted in Fig. 1. We note that even in the early phase when matter is extremely dense, opaque, and hot, strong line blanketing can be at work and the absorption in the UV may not be negligible and thus the real temperature of the blue component can be higher. In the first epoch at 0.5 d after the trigger, the peak of the blackbody is at much bluer wavelengths than the available photometry and cannot be constrained therefore in this case, we have only extrapolated the model to the NIR, after imposing the blackbody temperatures to be $\leq 10\,000$ K. For this reason, the *U*- and *B*-band KN template light curves start at 0.66 and not at 0.5 d after the trigger, like the other bands.

In order to maximize the possibilities of comparison with GRB counterparts down to the UV and up to the NIR regimes, we then modelled the UV and NIR extremes of the spectra, leaving untouched the rest of the spectral interval already covered. At the time of the X-shooter spectra (> 1.5 d), it is likely that the ejected matter becomes more transparent and absorption features start to dominate the spectra. Therefore, modelling the data with one or more blackbody components without considering absorption is not possible. However, given that we are only interested in expanding the spectral interval of the templates in the case of the X-Shooter spectra we have modelled the data with two power laws, one below 5000 Å and one above $21\,000$ Å (see Fig. 2). The best-fitting

models have been used to extrapolate the AT2017gfo flux down to 1500 Å and up to $26\,000$ Å. Finally, we have computed the best-fitting spectral models in the KN rest frame. For AT2017gfo, we have adopted the redshift $z_{\text{KN}} = 0.0098$ (Hjorth et al. 2017) that, with the assumed PLANCK cosmology, corresponds to a luminosity distance of $D_L = 43.7$ Mpc.

The result of this procedure is a set of spectral templates, covering the UV to NIR range, computed at different epochs between 0.5 and 10 d after the GW trigger. We then used these templates to produce rest-frame light curves of AT2017gfo for all the GRB filters as explained in the next section. In Fig. 3, we show a sample of light curves for few selected optical/NIR filters (see also Table A3), computed also assuming a luminosity distance of 40.7 Mpc, as found by Cantiello et al. (2018). It is clear that the peak of the optical emission lies in the first day after the trigger, while the NIR emission is almost constant during the first 6 d and dominates the emission after 2 d.

3.2 Comparison with short GRBs

To proceed with the AT2017gfo–short GRBs comparison, each short GRB flux F_ν measured at the time t_{GRB} was converted to a luminosity and, for each filter, a rest-frame light curve was built. In order to compare the AT2017gfo and GRB luminosity in the same frequency, we proceeded as follows. For each GRB of our sample, we have a set of filters used for the observations. Given a GRB at redshift z_{GRB} , for each filter X centred at the observed frequency ν_X , we computed an effective rest-frame filter X_{eff} centred at $\nu_{X,\text{eff}} = \nu_X \times (1 + z_{\text{GRB}})$. By integrating the AT2017gfo luminosity spectra taken at different epochs (t) over the effective rest-frame filter X_{eff} ,⁴ we were able to build a AT2017gfo luminosity light curve $L_{X,\text{eff}}(t)$ in the rest-frame filter X_{eff} , i.e. the same in which the GRB was observed.

With this procedure, we built a set of AT2017gfo luminosity light curves in the same set of filters used to observe a given GRB. In this way, we could proceed in a straightforward manner to the comparison of the luminosity of AT2017gfo and the GRB afterglow in each filter. Note that using the distance of 40.7 Mpc found by Cantiello et al. (2018), AT2017gfo would become fainter of a factor ~ 1.15 and therefore the luminosity ratios would change. However, this would not change qualitatively our conclusions.

4 RESULTS

In the following, we present the results obtained from the comparison in each filter of the AT2017gfo luminosity and those of the optical and NIR counterparts of our selected sample of short GRBs.

The GRB counterparts and AT2017gfo light curves in different bands are plotted as luminosity (left side) and apparent magnitude (right side) versus rest-frame time in Figs A1–A4. Note that several filters with similar wavelength have been grouped into a single one in the plots for visualization purposes, and that the filters quoted in each plot are the ‘effective’ ones, i.e. the observed filters shifted to the GRB rest frame (Section 3.2).

In order to avoid any model-dependent temporal extrapolation, in this work we limited the comparison to the short GRBs observations that fall in the sampled AT2017gfo temporal window (0.5–10.5 d in rest-frame). For this reason, for 13 short GRBs the comparison

⁴The effective rest-frame filter was obtained by multiplying the filter response matrix by $(1 + z_{\text{GRB}})$.

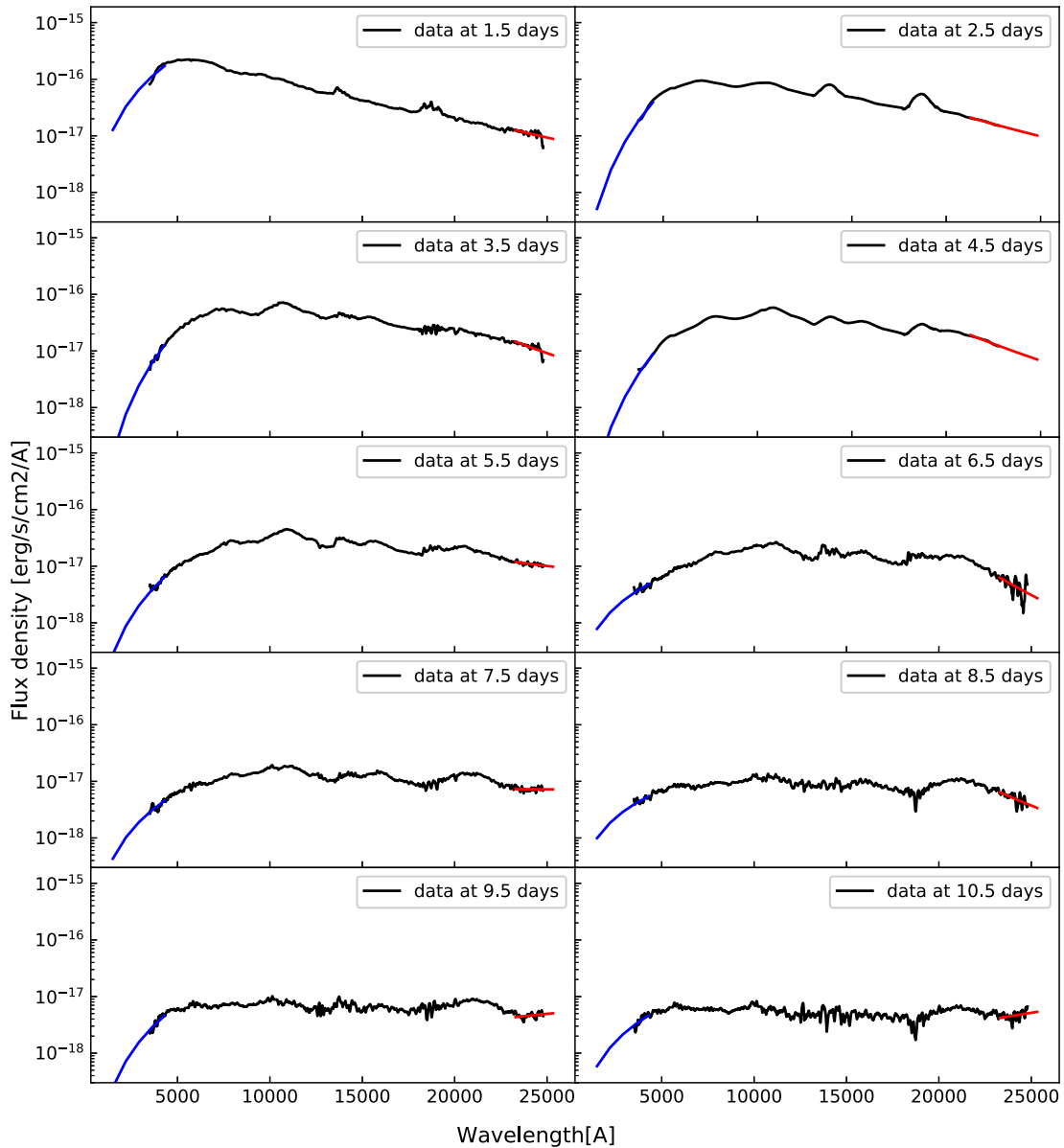


Figure 2. X-Shooter spectra between 1.5 and 10.5 d after the trigger (black) of AT2017gfo. The blue and NIR tails have been modelled with a power-law $F(\nu) \propto \nu^a$ (blue and red lines; see Section 3.1).

with AT2017gfo was not possible. However, we still show their light curves as illustrative examples of the magnitude range of AT2017gfo-like emission in comparison with those of the observed GRB counterparts (see Fig. A4). In the case of GRB 100206A, albeit not covered by the KN templates, the gap is negligible and the observations are clearly fainter than the KN template (see below Section 4.1). In Table A1, we quote the luminosity as well as the ratios between GRB counterpart and AT2017gfo luminosity in the spectral bands and at the time of the observations at which such comparison was possible.

On the basis of the luminosity ratios and on the temporal behaviour of the GRB counterpart luminosity, we built three main groups as described below (see Sections 4.1–4.3). The first group includes seven GRBs with a counterpart fainter than AT2017gfo in at least one filter. The light curves of these GRBs are shown in Fig. A1 and two examples are plotted in Fig. 4. The 19 short GRB counterparts brighter than AT2017gfo are plotted in Figs A2 and

A3. Moreover, we distinguish between the *blue* and *red* components, depending on whether the rest-frame effective wavelength is below or above 900 nm, respectively. In Table 2, we summarize the short GRBs that stand out for their properties.

4.1 Short GRBs with optical counterpart fainter than AT2017gfo

We find that in seven cases (namely GRBs 050509B, 050709, 061201, 080905A, 090515, 100206A, and 160821B), the luminosity of the optical counterparts is smaller than that of AT2017gfo in at least one filter. This is also true in the case of GRB 100206A, although the photometric monitoring ends before the temporal window of the light curve of AT2017gfo.

In the first part of Table 2, we report the rest-frame time after the GRB event (together with the effective rest-frame filters and wavelengths; see Section 3.2) in which we find that AT2017gfo

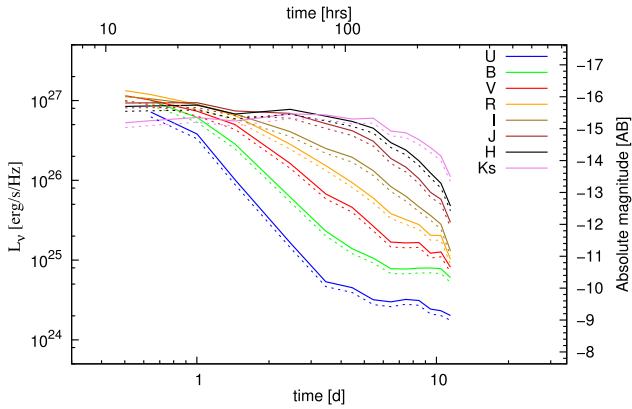


Figure 3. Rest-frame light curves of AT2017gfo in few selected filters (continuous lines; distance of 43.7 Mpc). The *U*- and *Ks*-band light curves were obtained by extrapolating photometry and spectroscopy to obtain a full coverage of the filter transmissions (see Section 3.1 and Table A3). The dashed line curves have been obtained assuming a distance of 40.7 Mpc as found by Cantiello et al. (2018).

Table 2. Summary of the GRB to KN luminosity ratios in the effective rest-frame filters (Section 3.2) of short GRBs that stand out for their properties (full Table in A1). The sample is divided between events fainter (first part of the table) and brighter (second part of the table) than AT2017gfo. GRBs with accurate redshift (Section 2.3) are quoted in bold.

GRB	Time ^a (h)	Band ^b (eff)	λ_{eff}^b (nm)	L ratio ^c GRB/KN	ID ^d	Com. ^e
050509B	21.2	$R_{f(1+z)}$	523	<0.3	Blue	–
	36.6	$R_{f(1+z)}$	523	<0.2	Blue	–
	52.2	$R_{f(1+z)}$	523	<0.7	Blue	–
050709	50.8	$I_{f(1+z)}$	681	0.8	Blue	S,KN
061201	29.8	$I_{f(1+z)}$	712	<0.3	Blue	–
	73.3	$I_{f(1+z)}$	712	<0.7	Blue	–
080905A ^f	12.8	$R_{f(1+z)}$	572	0.3	Blue	–
090515	17.8	$r_{f(1+z)}$	446	0.4	Blue	S
160821B	22.1	$r_{f(1+z)}$	539	0.9	Blue	S,KN
	78.1	$J_{f(1+z)}$	1081	0.5	Red	–
	102.8	$K_{f(1+z)}$	1863	0.9	Red	–
100206A	~10	$i_{f(1+z)}$	544	<1	Blue	–
050724	27.7	$I_{f(1+z)}$	628	6.0	Blue	S,MKN
	66.1	$I_{f(1+z)}$	628	2.4	Blue	–
	27.8	$R_{f(1+z)}$	510	9.1	Blue	–
060614	12.8	$R_{f(1+z)}$	570	16.9	Blue	S,KN
	143.8	$R_{f(1+z)}$	570	8.6	Blue	–
070714B	54.9	$R_{f(1+z)}$	333	263	Blue	MKN
070809	23.8	$R_{f(1+z)}$	435	3.4	Blue	KN
130603B	28.3	$r_{f(1+z)}$	462	1.3	Blue	KN
	164.7	$H_{f(1+z)}$	1218	3.0	Red	–
150101B	35.1	$r_{f(1+z)}$	552	2.1	Blue	KN
150424A	16.4	$r_{f(1+z)}$	481	15.2	Blue	S
	12.4	$J_{f(1+z)}$	964	37.2	Red	–

^aRest-frame time.

^bRest-frame effective band and effective wavelength (Section 3.2).

^cGRB optical counterpart to AT2017gfo luminosity ratio.

^dThis column indicates if the effective wavelength is below (blue) or above (red) 900 nm.

^e‘S’ = evidence of shallow decay from this work; ‘KN’ = evidence of KN from the literature; ‘MKN’ = evidence of magnetar-powered KN from Gao et al. (2017).

^fIn the case of GRB 080905A, the decay index of the optical/NIR light curve is $\alpha = 0.4 \pm 1.3$ between 7 and 16 h after the trigger (rest frame), preventing us to constrain any anomalous shallow decay.

was fainter than the optical/NIR counterpart of the GRB by a factor quoted in the fifth column as the luminosity ratio. We note that for two of these seven short GRBs (namely GRB 050709 and GRB 160821B), a KN emission has been invoked in the literature (Jin et al. 2016, 2018; Kasliwal et al. 2017a; Lamb et al. 2019; Troja et al. 2019). These GRBs have been labelled in the last column of Table 2 with ‘KN’. The cases with evidence of magnetar-powered KN (see Gao et al. 2017) have been labelled with ‘MKN’. Moreover, for three GRBs we find evidence of a shallow decay not consistent with the standard fireball model (see next section). The latter ones are labelled with ‘S’ in Table 2. For all the short GRBs belonging to this group, we could probe the *blue* KN component and constrain its luminosity within a range of 0.2–1 times the AT2017gfo luminosity. In the NIR, only the red counterpart of GRB 160821B is fainter (0.4–0.9 times) than At2017gfo (Table 2).

4.2 Short GRB counterparts with shallow decay

A KN is expected to show a shallow evolution close to its maximum brightness. Therefore, it can be distinguished from the standard afterglow decay, which at the typical observing time (i.e. > minutes after the burst) has a constant power-law decay (e.g. Sari, Piran & Narayan 1998; Sari, Piran & Halpern 1999; Zhang & Mészáros 2004; Zhang et al. 2006).

KN peak brightness is typically estimated around a few days after the merger assuming simple one-component modelling and fiducial values (e.g. Metzger et al. 2010). However, according to more sophisticated models (e.g. Radice et al. 2018), the KN maximum brightness can be as early as <0.1 d, depending on the nature of the central remnant (i.e. if a BH or an NS is generated, see their fig. 28). Thus, we considered as possible evidence of a KN a shallow evolution in the optical counterpart of the short GRBs that can happen from a few hours after the burst up to a few days. Our simple method of KN identification is effective only near the KN peak epoch. In fact, it is not suited to find events where the KN is dominating but its decay is too steep to be distinguished from an afterglow (for example see the case of GRB 150101B in Section 4.3). A shallow decay simultaneous to a X-ray plateau can possibly indicate the presence of an MKN (see Gao et al. 2017), although other explanations are possible (e.g. Mangano et al. 2007). Therefore, we also describe the simultaneous behaviour of the X-ray light curve.

Under the reasonable assumption of a slow cooling regime for the electrons producing the observed afterglow radiation (see Sari et al. 1998, 1999), the predicted shallowest flux decay power-law index is $\alpha = 3(p - 1)/4$ where p is the power-law index of the electron energy distribution. In this context, using a minimal electron index $p = 2$ in the slow cooling regime, we considered a decay to be anomalously shallow when $\alpha < 0.75$. We computed the decay index α for all GRBs for which two or more observations were available. We note that the flattening in the GRBs 071027 and 061006 is due to the contribution from the host (D’Avanzo et al. 2009), and thus they are not considered here.

In seven cases, we have found a suspicious shallow decay that can indicate the presence of a KN emission dominating over the afterglow component. We quote them in Table 2. Note that in all cases, we could measure a shallow decay only in the optical filters, i.e. in the regime of the blue component. The results are summarized in Table 3. In Fig. 5, we compare the estimated decay indexes with those of AT2017gfo, computed assuming a power-law evolution between consecutive template epochs (Fig. 3). Note that the decay index of the KN is always smaller in the *J* band than in optical bands

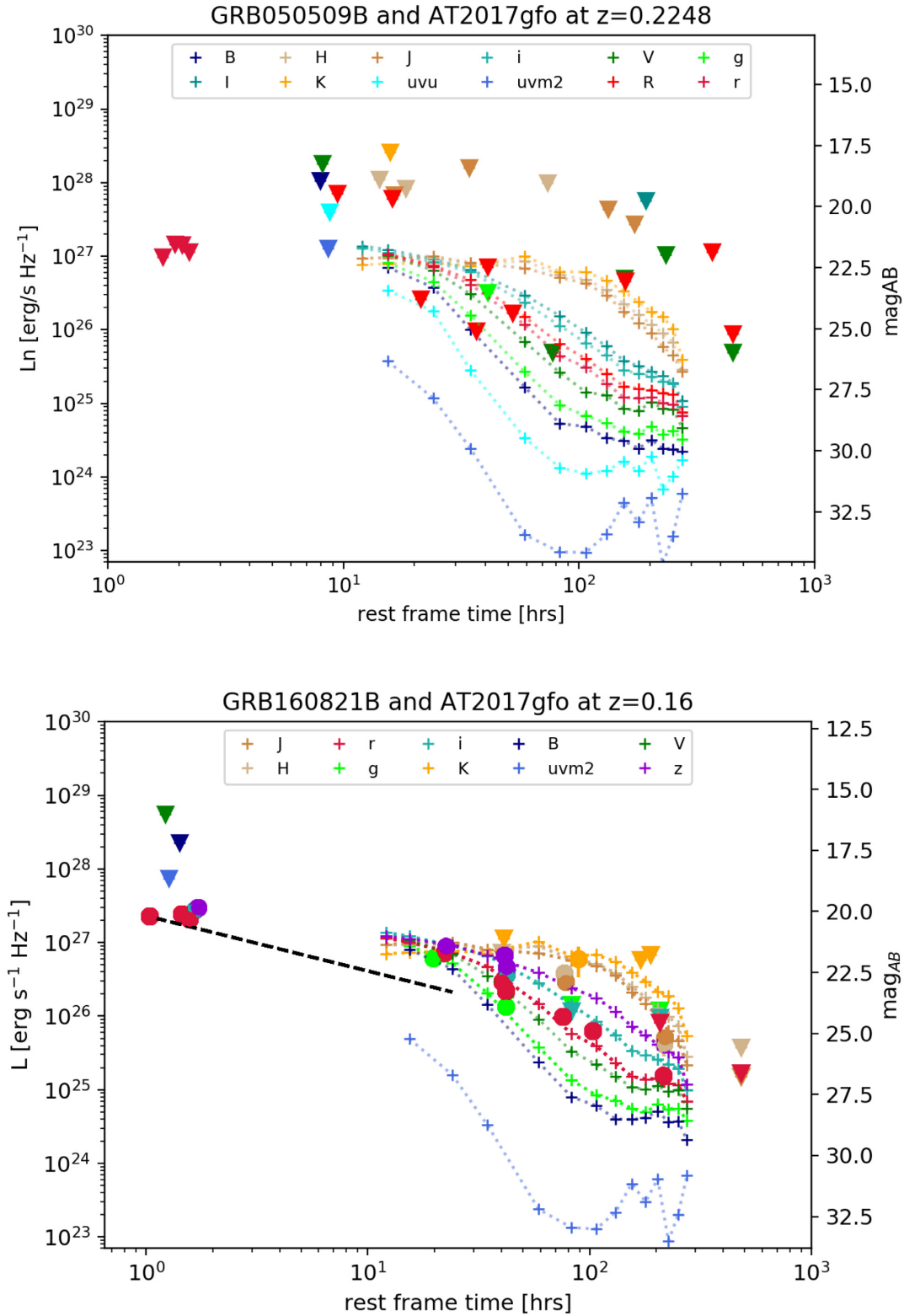


Figure 4. Two examples of short GRBs for which the optical counterpart luminosity (circle for a detection and triangle for an upper limit) is fainter than AT2017gfo luminosity (dotted lines with crosses) in at least one effective rest-frame filter (see Section 3.2 for effective rest-frame filter definition). See Fig. A1 for the full sample of short GRBs with similar properties. Note that GRB 160821B (*lower panel*) shows evidence of a temporal decay index lower than the shallowest index predicted by the fireball model (i.e. $\alpha = 0.75$, see Section 4.2, black dashed line). If this anomalous shallow decay is due to an emerging KN emission, its NIR luminosity is a factor of 1.2–2 fainter than AT2017gfo at epochs later than 3 d after the merger time in *r* and *J* bands (see Table 2).

Table 3. Summary of the short GRBs with evidence of an anomalous shallow decay and/or with a claimed KN in the literature. GRBs with well-defined redshift (Section 2.3) are quoted in bold and represent our golden sample (Section 5.2).

GRB	Band ^a (eff)	α ^b	t_{start} ^c (h)	t_{end} ^c (h)	Com. ^d
050709	$I_{(1+z)}$	0.6 ± 0.2	50.7	115.8	KN, S
	$I_{(1+z)}$	1.2 ± 0.1	115.8	202.1	
050724	$R_{(1+z)}$	<0	4.4	9.4	MKN, S
	$R_{(1+z)}$	1.5 ± 0.1	9.4	27.8	
060614	$R_{(1+z)}$	0.2 ± 0.1	1.0	10.0	KN, S
090515	$r_{(1+z)}$	0.1 ± 0.1	1.2	17.8	S
150423A	$r_{(1+z)}$	0.4 ± 0.2	0.4	1.7	S
150424A	$R_{(1+z)}$	0.09 ± 0.03	1.2	10.1	S
160821B	$R_{(1+z)}$	0.0 ± 0.1	1.0	1.6	KN, S
	$R_{(1+z)}$	0.40 ± 0.03	1.6	22.1	
070714B	$R_{(1+z)}$	1.0 ± 0.3	12.3	54.9	MKN
130603B	$H_{(1+z)}$	1.6 ± 0.1	10.7	164.7	KN
	$R_{(1+z)}$	2.7 ± 0.1	10.9	28.3	
150101B	$r_{(1+z)}$	1.0 ± 0.3	35.1	56.1	KN

^aRest-frame effective band (Section 3.2).

^bDecay index ($F_{\nu}(t) \propto t^{-\alpha}$).

^cRest-frame time interval within which α was computed.

^d‘S’ = evidence of shallow decay from this work; ‘KN’ = evidence of KN from the literature; ‘MKN’ = evidence of magnetar-powered KN from Gao et al. (2017).

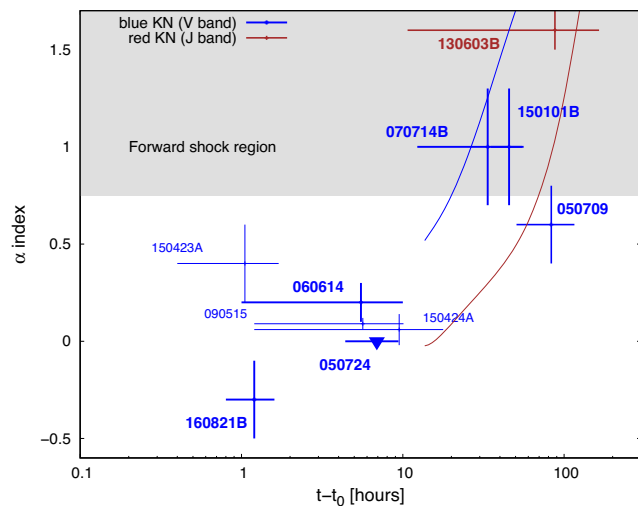


Figure 5. The decay indices of the GRB optical counterparts during the shallow decay. See Table 3. The short GRBs labels are coloured following the band in which the decay index was computed. Upper limits are indicated as downward triangles. GRBs in the golden sample are highlighted in bold. The horizontal line indicates the lowest possible decay index predicted by the afterglow theory ($\alpha = 0.75$; see Section 4.2). The curves are the smoothed splines of the decay indices of AT2017gfo in the V and J bands, from top to bottom, computed in the 13 epochs. These are derived by computing the decay between two epochs in the template light curves shown in Section 3 with a time-step of 0.5 d.

thus reflecting the expected smoother evolution in the red band with respect to the blue one.

In the following, we discuss in more detail these bursts. Note that three of them (GRBs 050709, 090515, 160821B) are also part of the first group, i.e. those GRBs with optical counterparts fainter than AT2017gfo. According to AT2017gfo templates (Fig. 3), the blue

component dominates during the first 24 h, therefore we first list those short GRBs for which we measured a shallow decay before 1 d. We include also those short GRBs for which we measured a shallow decay at epochs earlier than the first AT2017gfo observation (i.e. before ~ 11 h).

(i) **GRB 050724.** Its early R -band light curve is rising between 5.6 and 11.8 h after the trigger (4.4 and 9.4 h in rest frame), with $\alpha \sim -0.5$. Simultaneous X-ray and radio data show a similar trend. Gao et al. (2017) interpreted this behaviour as evidence for a KN powered by a magnetar. We find that, if it were an emerging KN, its blue component is brighter than AT2017gfo up a factor 9 and 6 in R and I bands at ~ 28 h (rest frame), respectively. This factor decreases to ~ 2.4 at ~ 66 h.

(ii) **GRB 060614A.** In this case, the R -band light curve shows a clear shallow decay phase between 1.5 and 11 h (1 and 10 h in rest frame) simultaneous with an X-ray plateau feature, with a brightening peaking at ~ 4 h after the trigger. In this case, the detected luminosity are a factor of ~ 16 larger than the R -band luminosity of AT2017gfo at ~ 12.8 h after the trigger. Jin et al. (2015) and Yang et al. (2015) found a KN component for this burst at more than ~ 3 d after the trigger from an optical excess in the afterglow. At this time we find no clear evidence of an optical shallow decay (see Section 5.2.1).

(iii) **GRB 090515.** In this case, the r -band light curve has a decay index $\alpha \sim 0.1$ between 1.7 and 25 h after the trigger (1.2 and 17.8 h in rest frame). Moreover, a very late ($\sim 10^3$ h) deep upper limit confirms that no emission from an underlying host is affecting the early data. The X-ray afterglow is very weak and no data are available for a comparison after the first hour. If a KN is emerging from the afterglow emission, it is fainter than AT2017gfo by a factor of 2.3 at ~ 18 h after the trigger. Note that this case was already presented in Section 4.1.

(iv) **GRB 150423A.** This burst shows a shallow decay behaviour in the i and z bands, with index $\alpha = 0.4 \pm 0.2$ in the r band before 4 h after the trigger (1.7 h in rest frame). The temporal mismatch with the AT2017gfo light curves prevents us from performing a more quantitative comparison. We note that during the same time interval, the X-ray light curve is much steeper ($\alpha_x \sim 0.96 \pm 0.07$), thus suggesting a different origin with respect to the optical counterpart.

(v) **GRB 150424A.** In this case, the r -band light curve has an atypical shallow decay with index $\alpha \sim 0.1$ between 1.6 and 13 h after the trigger (1.2 and 10.1 h in rest frame), simultaneous with an X-ray plateau feature. If a KN is the dominant component, its blue component is brighter than AT2017gfo by a factor of ~ 15 at ~ 16.4 h after the trigger (rest frame), i.e. at the end of the shallow phase. At the same time in the J, H bands, the light curve is brighter than AT2017gfo by a factor ~ 30 and falls to ~ 2.3 times brighter at ~ 124 h after the trigger.

(vi) **GRB 160821B.** For this event, the presence of a KN emission was claimed by Troja et al. (2019). In this case, the R -band counterpart shows a brightening at ~ 1 h after the trigger ($\alpha \sim -0.3$), which then steepens to $\alpha \sim 0.9$ between 1 and 86 h after the trigger (1.6 and 74.5 h in rest frame). A very weak X-ray afterglow possibly shows evidence of a plateau lasting ~ 1 d after the burst. If an underlying blue KN component is peaking at ~ 1 d after the trigger, the KN is fainter than AT2017gfo by a factor in the range 1.1–2.5 (see Table 2). As also noted by Troja et al. (2019), the late J - and H -band light curves have a behaviour similar to that of KN170817, but have a decay index larger than one (see also Lamb et al. 2019). This case was already presented in Section 4.1.

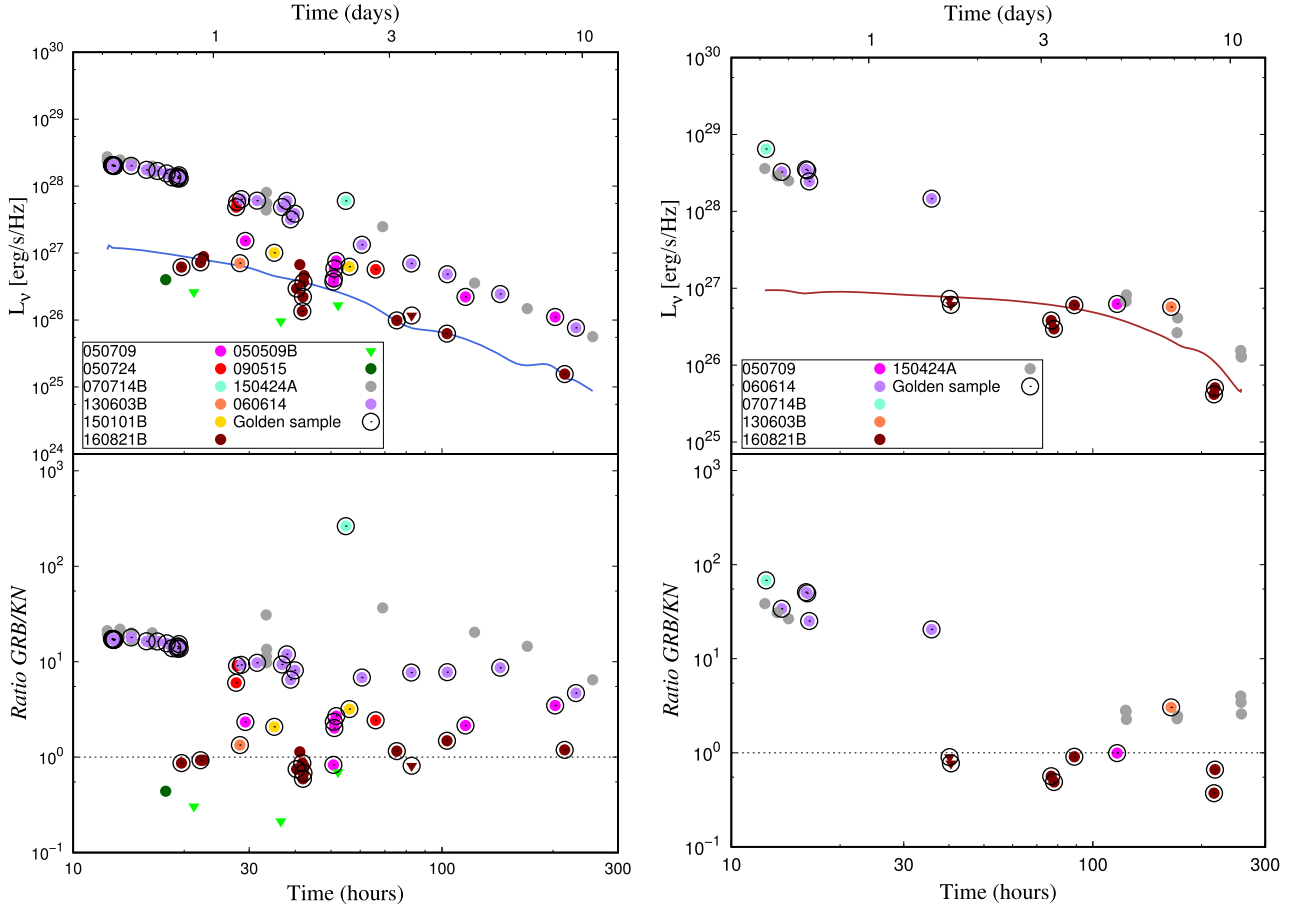


Figure 6. Luminosity (*top*) and luminosity ratios (*bottom*) of GRB and AT2017gfo versus time from merger for the blue (*left*) and red (*right*) spectral bands (blue: <900 nm, red: >900 nm). Data are taken from Table A1 after shifting the effective wavelengths of the filter bands to the rest-frame value. Upper limits are indicated as downward triangles and plotted only when below AT2017gfo luminosity. Short GRBs with anomalous shallow decay are highlighted with different colours, including those without a well-defined redshift. Bursts that belong to our golden sample are highlighted with a black circle (see Section 5.2). The blue and red solid lines in the top panels indicate the AT2017gfo luminosity at 800 and 1600 nm wavelength, respectively.

Below we describe the short GRB for which we measured a shallow decay at more than 24 h after the trigger.

(i) **GRB 050709A.** For this burst, the presence of a KN was claimed by Jin et al. (2016). In this case, the *R*-band light curve is very shallow with $\alpha \sim 0.7$ between 59 and 134 h after the trigger (51 and 116 h in rest frame) and no straightforward comparison with X-ray data was possible due to the lack of enough statistics in the data (Fox et al. 2005). From the comparison with AT2017gfo, if the claimed KN signature is real, then its luminosity is comparable within the uncertainties in the *K*, *I*, and *V* bands, although afterglow contamination is still possible. This case was already presented in the previous section.

4.3 Short GRBs with known kilonova candidates

In few cases, a KN component has been found in the optical/NIR GRB counterpart light curves and published in the literature. Two of them (GRBs 050709 and 160821B) have an optical counterpart fainter than AT2017gfo and are already part of the first group in Table 2. Others (namely GRBs 050724, 060614, 070714B, 070809, 130603B, and 150101B) have an optical/NIR counterpart brighter than AT2017gfo and we report them in the second part of Table 2.

Gao et al. (2017) found evidence of KN in GRBs 050724 (see Section 4.2), 061006, and 070714B by modelling the X-rays and optical light curves with an MKN model. However, as we noted in Section 4.2, D’Avanzo et al. (2009) found that the optical light curve of 061006 is dominated by the host galaxy, thus we have included only GRB 050724 and GRB 070714B in our analysis (see Table 3). In case of 070714B, we cannot identify a shallow phase, but Gao et al. (2017) found an MKN peaking at ~ 2 d (observer frame; ~ 1 d in rest frame). During the time when this component is dominating there are two photometric epochs, one at ~ 11 h (just earlier than the first AT2017gfo photometric measurement) and one at ~ 55 h. During the first epoch, the blue counterpart is clearly more than 10 times brighter than AT2017gfo, and the ratio increases to ~ 260 times at the second epoch.

In the case of GRB 070809, recently Jin et al. (2020) discovered a KN in its optical light curve. Unfortunately, its redshift is not well determined and therefore it cannot be used to constrain the optical luminosity of the KN with confidence.

For GRBs 130603B and 150101B, a KN component was claimed in the literature (Tanvir et al. 2013). The KN was detected with an observation taken ~ 7 d after the burst in the *H* band (Tanvir et al. 2013). At that time, its luminosity in the same band is ~ 3 times brighter than AT2017gfo (see Fig. A3).

In the case of GRB 150101B, the r -band light curve has a decay index $\alpha \sim 1$ between 35 and 56 h after the trigger which is above the shallow decay limit. Troja et al. (2018a) show that this light curve is compatible with the late evolution of the blue component of AT2017gfo, well after the peak emission. We find that if a blue KN is the dominant component, it is brighter than AT2017gfo by a factor ~ 2 at ~ 35 h after the trigger. Moreover, the deep and late upper limits confirm that no emission from an underlying host is affecting the early data.

5 DISCUSSION

In the following, we first discuss those GRBs that are fainter than AT2017gfo, without considering those with uncertain redshift. Afterwards, we will discuss the cases with shallow decay or with a claimed KN, by defining a golden sample of GRBs with accurate redshifts and by using their luminosity to constrain that of AT2017gfo-like blue and red KN components.

5.1 Upper limits to AT2017gfo-like kilonovae

In the previous section (Section 4.1), we show that in seven cases an AT2017gfo-like emission could have been detected since its expected luminosity is well above the observed optical counterpart luminosity (see Tables 2 and A1). In particular, we note that in two cases (GRBs 050509B and 061201) if a KN was present, it should be less luminous than AT2017gfo up to more than a factor of 5 for the blue component (see also Gompertz et al. 2018). In the following, we will consider only those with accurate redshift determination (see Section 2.3), which are GRB 050509B, 050709, 100206A, and 160821B. The counterpart luminosity of these four GRBs enables us to robustly set constraining upper limits to a possible underlying KN component that is fainter than AT2017gfo (see also Dichiarà et al. 2020).

In Fig. 6, we compare their optical and NIR counterpart luminosity with the blue and red component of AT2017gfo (the spectral bands of the blue and red component have been defined in Section 4). In the blue component spectral band, the strongest constrain is given by GRB 050509B that is more than 5 times fainter than AT2017gfo ~ 35 h after the trigger. GRBs 100206A and 050709 are marginally fainter and still comparable in luminosity to AT2017gfo at 12 and ~ 50 h after the trigger, respectively.

For the red component, GRB 160821B was fainter than AT2017gfo, although its blue component has similar luminosity. The deepest and earliest constraint is a factor ~ 2 fainter than AT2017gfo at ~ 1000 nm at ~ 78 h after the burst, close to the actual NIR peak of AT2017gfo, indicating that in this case the red KN is at least partially suppressed. Intriguingly, in the bottom right panel in Fig. 6 we show that there are no NIR upper limits below AT2017gfo luminosity after ~ 50 h (see also Section 5.2.1). The same is not true in the left-hand panel, where upper limits exist below AT2017gfo luminosity level, thus possibly suggesting a larger range of luminosity for the blue counterpart with respect to the red one.

5.2 Golden sample of GRBs with kilonova candidates

Past evidence of KN emission was found in the GRB optical counterparts of six short GRBs (050709A, 060614A, 080503, 130603B, 150101B, and 160821B; see Section 1 and references therein). In addition to those, there are the magnetar-powered kilonovae identified by Gao et al. (2017; GRBs 050724, 070714B).

In all cases but GRB 080503 the redshift is well defined. Therefore, we define a golden sample that includes all seven GRBs with KN candidates claimed in the literature that have accurate redshift.

5.2.1 Interesting extreme events

We define ‘extreme’ events those cases in our golden sample that are more than 10 times brighter or fainter than AT2017gfo either in the blue or in the red bands. We find two cases with a bright blue counterpart, namely GRBs 060614 and 070714B.

Concerning GRB 060614, in this work we show that its optical light curve has a shallow decay until 10 h after the trigger (rest frame; see Section 4.2) and the blue counterpart is 17 times brighter than AT2017gfo at 13 h (i.e. at the end of the shallow decay). We note that a KN has been found by Yang et al. (2015) but dominating 3 d after the GRB, with a peak in the infrared (Jin et al. 2015). In Mangano et al. (2007), the early optical behaviour of GRB 060614 is explained as the counterpart of the plateau observed in X-rays. However, the similarity of the optical and X-ray light curves of GRB 060614 with GRB 050724 (see also Fig. A2), for which an MKN was claimed by Gao et al. (2017), may support the blue component interpretation of the early emission for both cases.

The blue counterpart of GRB 070714B is between 10 and ~ 260 times brighter than AT2017gfo between 11 and 55 h (Section 4.3). During this time, Gao et al. (2017) propose that an MKN is dominating. They show that the peak bolometric luminosity of MKNs is $\gtrsim 10$ times more luminous than other kilonovae like the one associated with 050709, which we find more similar to AT2017gfo. This is also the case for the MKN associated GRB 050724, which instead is more similar to AT2017gfo in our analysis (see Section 5.2). However, the proposed MKN peaks at ~ 0.5 d, i.e. too early for a comparison with AT2017gfo templates, and afterwards it decays rapidly. Therefore, our analysis cannot constrain the peak bolometric luminosity.

In the NIR band, all the kilonovae detected (GRBs 050709, 130603B, 160821B, Section 4.3), are no more than 3 times brighter or fainter than AT2017gfo during the time where the red KN dominates (after 1 d, see Tanvir et al. 2013; Jin et al. 2016; Lamb et al. 2019). Moreover, as we noted already in Section 5.1, there are no upper limits in the NIR comparable to AT2017gfo luminosity after ~ 2 d. In other words, in all cases when observations comparable to AT2017gfo NIR emission exist the KN counterpart has been detected. This suggests that all red KN detected so far have similar luminosity, although we are aware that the numbers are not high enough for a meaningful statistic.

5.3 Interesting events without accurate redshifts

The redshifts of GRBs 090515 and 150424A are not well defined (see Section 2.3), nevertheless they can be useful to constrain the luminosity of AT2017gfo-like kilonovae since both show evidence of shallow decay that can suggest the presence of a KN component. In particular, GRB 090515 is the most interesting because the blue component have a well-constrained luminosity 2.3 times fainter than AT2017gfo (Fig. 5). If its redshift is correct, together with 050509B it would provide the strongest and earliest constraints to the blue component of an AT2017gfo-like KN (Fig. 6).

GRB 150424A has a shallow decay but its blue component is ~ 15 – 40 times brighter than AT2017gfo in the optical (Fig. 6). During the same time interval, the X-ray light curve shows evidence of a plateau feature. This could be an MKN similar to GRBs

050724, 070714B, and 060614 (Section 5.2.1), although Knust et al. (2017) found that energy injection from a down spinning magnetar can explain X-rays, optical, and NIR data without invoking a KN.

A more detailed analysis is needed to separate the KN and afterglow components modelling together both optical and X-ray data (see e.g. Gao et al. 2017; Jin et al. 2020; Lamb et al. 2019). Unfortunately, in case of GRB 090515 the X-ray data are weak and detected only during the first hour.

5.4 Interpreting the large range of luminosity

AT2017gfo is the only KN that has been very well sampled and studied so far, but it is a one-of-its-kind example and other kilonovae may differ for their evolution and colours. Providing a theoretical explanation for kilonovae 10 times brighter than AT2017gfo is beyond the scope of this paper. However, in the following we describe the possible causes to the large range in luminosity that we have found.

According to the most accredited model (e.g. Mooley et al. 2018b; Ghirlanda et al. 2019), AT2017gfo was observed ~ 15 deg off-axis while here we are comparing it with likely on-axis events (see also Bulla et al. 2019; Mandel 2018). A KN luminosity gradient at a given wavelength is expected between the polar and the equatorial direction of the binary plane system, and many parameters including its magnitude depend on the fate of the central remnant (e.g. Kasen et al. 2017; Radice et al. 2018). According to recent numerical computations (see e.g. fig. 24 in Radice et al. 2018), in the case of a binary NS system (BNS) promptly forming a BH the result is an overall decrease of luminosity by less than a factor 2 (i.e. ~ 0.5 mag) in the polar direction with respect to the equatorial one. Accounting for an off-axis inclination like AT2017gfo, then the polar emission should be less than 2 times fainter. This is not enough to explain the low-luminosity ratio of those GRBs with optical counterpart fainter than AT2017gfo (Table 2). In the case of a hyper massive NS (HMNS) or a stable NS being formed, then the polar luminosity should increase in the rest-frame g and z bands by a factor of less than 1.5 with respect to the equatorial direction (i.e. a decrement of $\Delta g \leq 0.4$ mag and $\Delta z \leq 0.2$ mag). Again, this factor is not high enough to explain the measured large luminosity ratios for the peculiar events we describe in Section 5.2.1. We conclude that, in the prompt BH formation case we cannot explain the measured luminosity gradient for any viewing angle and even assuming a central HMNS formation before the collapse to a BH, the viewing angle correction factors are not large enough to recover the observed luminosity gradients (Table 2).

A possible solution to explain the faint emission of the KN associated with the seven GRBs for which the optical counterpart was fainter than AT2017gfo may invoke not only a different viewing angle but also a different progenitor, i.e. NS–BH instead of BNS, where larger opacities are expected with respect to an NS–NS merger case (Kasen et al. 2015; Metzger 2017; Barbieri et al. 2019). Although in the most dramatic cases lower masses and velocities of the ejecta can play an important role (e.g. Dichiaro et al. 2020), any further investigation is beyond the scope of this paper.

On the other side, a possible explanation for the largest luminosity ratios may invoke the presence of a long-lived NS remnant that can alter the KN luminosity. In this case, its spin-down emission could illuminate the ejecta on time-scales much longer (up to hours or even more) than the typical time-scale of baryon wind ejection and neutrino irradiation (less than few seconds), effectively increasing the ejecta kinetic and thermal energy and thus potentially altering

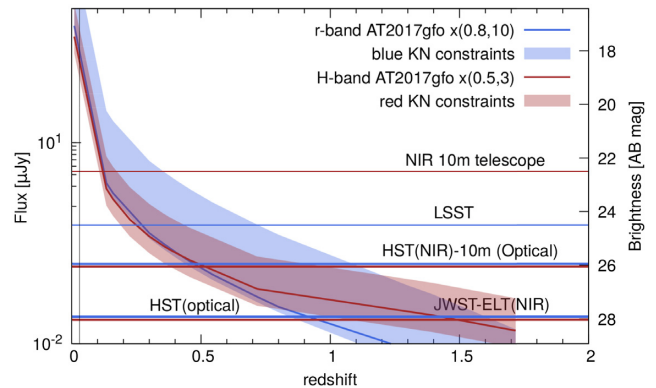


Figure 7. Peak brightness of AT2017gfo in the r (blue) and H (red) bands at different redshifts, within the constraints we derived for an AT2017gfo-like KN from the golden sample. The redshift range is limited at $z \sim 2$ at which ET will be able to observe a GW signal from a merging BNS. The vertical line is the aLIGO/AVirgo detection limits for a BNS event. The horizontal lines are different detection limits for different class of telescopes with an exposure time of 10 min.

the brightness of the corresponding KN (e.g. Metzger & Piro 2014; Gao et al. 2017).

A highly magnetized millisecond pulsar (a magnetar) has been previously proposed to explain the plateaus observed in the X-ray light curves of GRBs, where the magnetar loses energy via dipole radiation and thus provides the energy to sustain the X-ray plateau phase (Zhang & Mészáros 2001; Yu, Zhang & Gao 2013; Metzger & Piro 2014; Siegel & Ciolfi 2016a, b). Note that an X-ray plateau was found in the light curves of GRBs 060614A (Mangano et al. 2007; Stratta et al. 2018b), and 150424 (Knust et al. 2017) that show a blue component brighter than AT2017gfo. Therefore, it is possible that what we observed in these cases was a BNS merger exploding as a short GRB with a bright X-ray plateau and an luminosity-enhanced blue KN, leaving a magnetar as the final remnant of the merger, similarly to what proposed by Gao et al. (2017) for GRB 050724.

5.5 Future perspectives for high-redshift events

In the following, we want to investigate up to which redshift a KN can be followed up, considering the current and future optical and NIR facilities. In doing so, we do not consider the challenge to search and identify a KN within the error boxes given by the GW detectors (e.g. Brocato et al. 2018).

In Fig. 7, we show the maximum brightness of AT2017gfo in the observed r band (at 12 h in the rest frame) and H band (at 58 h in the rest frame) up to the redshift at which the future Einstein Telescope (ET; Sathyaprakash et al. 2012) will be able to observe a GW signal from a merging BNS ($z \sim 2$). In light of the results from Section 5.2, and conservatively assuming that the blue KN is brighter up to 10 times AT2017gfo, we can constrain the peak luminosity of the blue KN between 0.8 and 10 times that of AT2017gfo and for the red component between 0.5 and 3 times. These constrain identify blue and red coloured regions in Fig. 7. We put a lower limit to the 3σ detection with the current largest ground-based and orbiting telescopes dedicated to the characterization of the source: e.g. VLT, LBT ($r = 26$, $H = 23$ mag in the AB system), and the *Hubble space telescope* (HST) along with the forthcoming LSST (Ivezic et al. 2019; $r = 25$) and ELT (Spyromilio et al. 2008) ground-based telescopes and the JWST (Gardner et al. 2006) space telescope ($H \sim 28$ mag, AB system) assuming 10 min exposure time (see also

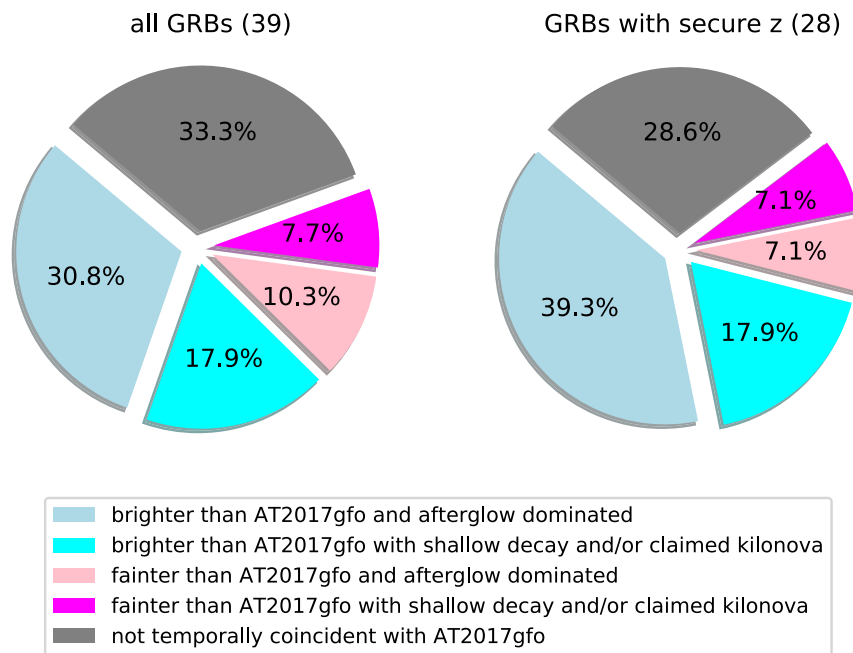


Figure 8. Pie chart summary of analysed short GRBs with optical counterpart brighter, or fainter in at least one filter, than AT2017gfo, and with claimed evidence of kilonovae and/or evidence of shallow decay. We also show all short GRBs with no evidence of KN or shallow decay, that we call *afterglow dominated*, and those with no data in the temporal window where AT2017gfo was sampled, that we call *not temporally coincident with AT2017gfo*.

Maiorano et al. 2018). An AT2017gfo-like KN would be detectable up to redshift 0.5 in the optical and 0.2 in the NIR by ground-based very large telescopes. The *JWST* will be able to detect AT2017gfo at redshift larger than one.

From Fig. 7, we note that a AT2017gfo-like KN would be brighter in NIR bands at redshift larger than ~ 0.5 , but only the *JWST* or the ELT would be able to detect this emission. Note that the current largest telescopes are able to detect the brightest AT2017gfo-like blue kilonovae above $z = 1$, a distance at which only *HST* is able to detect the brightest red kilonovae. The situation will improve when, due to *JWST* and ELT, we will be able to detect a KN up to $z \sim 0.7$ – 1.6 for the blue component and $z \sim 1$ – 2 for the red component (Fig. 7). This shows that follow-up of GRB/kilonovae with large-sized ground-based telescopes and space observatories at redshifts beyond that of AT2017gfo is possible, although in most cases it can be difficult to distinguish the GRB afterglow from the KN component.

Again, we stress that the real challenge will be to search and identify a KN within the error boxes given by the GW detectors. Distant GW sources ($z > 0.5$) will be discovered only with interferometers of third generation as ET and will be localized within several thousands square degrees with a single interferometer and within few tens of square degrees with three detector network (e.g. Chan et al. 2018). Therefore, only the association with a GRB will permit to localize high-redshift kilonovae with enough accuracy. This can be provided by future space-based GRB dedicated missions as for example THESEUS (Amati et al. 2018; Rossi et al. 2018a; Stratta et al. 2018a).

6 SUMMARY AND CONCLUSIONS

The discovery of GW170817 and GRB 170817A has provided the first direct evidence of the association of at least a fraction of short GRBs with binary NS merging systems. It also provided the most compelling evidence that KN emission may be an additional

component in sGRB optical/NIR afterglows. Motivated by this discovery, we have searched for AT2017gfo-like KN emissions in the optical/NIR light curves of 39 short GRBs with known redshift, using optical and NIR rest-frame light curves obtained from the spectroscopic and photometric data set of AT2017gfo.

In addition to past works, due to the large spectral coverage of our data sample, we were able to confirm the presence of a significant KN luminosity gradient for both the blue and red components. Our main results and conclusions are summarized in Fig. 8 and below:

(i) *We find robust evidence that not all short GRBs are associated with a AT2017gfo-like KN.* Indeed, we find seven events in which the GRB optical counterpart is less luminous than AT2017gfo in at least one filter (pink slices in Fig. 8). For these cases, if an AT2017gfo-like KN was present, it should have been detected. In particular for two GRBs with accurate redshift (050509B and 061201), the optical counterpart luminosity is fainter than AT2017gfo by a factor up to >5 for the blue component (see Fig. 6 and Table 2).

(ii) *We find evidence for a significant KN luminosity gradient for the blue component.* In 7 per cent of the cases with well-defined redshift (GRBs 050709 and 160821B), the kKNluminosity is fainter than AT2017gfo (violet slice in Fig. 8) while 18 per cent is brighter (bright cyan slice), providing evidence for a luminosity range of $\sim [0.6$ – $17]$ times the AT2017gfo luminosity for the blue component and more than 200 times in the case of the claimed magnetar-powered KN of GRB 070714B. (see Fig. 6 and Table 2). These percentages become 8 per cent (fainter) and 20 per cent (brighter) if we consider all the sample (i.e. also those GRBs with not well-defined redshift). As noted by others, a different observer angle is not sufficient to explain the measured luminosity range (e.g. Gompertz et al. 2018), and the central remnant can play a role (e.g. Metzger et al. 2018; Ascenzi et al. 2019). In particular, it is possible that if a magnetar forms after the merger even for a short time, it can inject energy in the blue KN emission (e.g. Gao et al. 2017).

(iii) *We find evidence for a similar KN luminosity for all kilonovae detected in the NIR (the red component).* In three cases (GRBs 050709, 130603B, 160821B), the KN is detected in the NIR after ~ 2 d, and it is less than a factor $\sim [0.5-3]$ times the AT2017gfo luminosity. Although the numbers are small, this suggests that the red component is similar in luminosity to AT2017gfo.

By taking into account a conservative range of blue luminosity for the KN, we estimate up to which redshift the KN peak brightness can be detected with current and future facilities. We find that for example with the ELT and *JWST* we will be able to follow-up a KN with redshift $z \sim 1-2$ (Fig. 7). The precise sky localization for the KN follow-up will be provided by the associated GRB and afterglow that will be detected by future space-based GRB dedicated missions as for example THESEUS.

ACKNOWLEDGEMENTS

The authors thank the anonymous referee for a very constructive report. We thank D. Radice for useful discussion about the KN models, and G. Raimondo for valuable suggestions. AR acknowledges support from INAF project ‘Premiale LBT 2013’. We acknowledge support from INAF for the PRIN INAF 2016 project ‘Toward the SKA and CTA era: discovery, localization, and physics of transient sources’ (P.I. M. Giroletti). We also acknowledge INAF financial support of the project ‘Gravitational Wave Astronomy with the first detections of adLIGO and adVIRGO experiments’. This work made use of the Weizmann interactive supernova data repository – <http://wiserep.weizmann.ac.il>. This research has made use of the NASA/IPAC Infrared Science Archive, which is operated by the Jet Propulsion Laboratory, California Institute of Technology, under contract with the National Aeronautics and Space Administration.

REFERENCES

- Abbott B. P. et al., 2017a, *Phys. Rev. Lett.*, 119, 161101
 Abbott B. P. et al., 2017b, *ApJ*, 848, L12
 Abbott B. P. et al., 2017c, *ApJ*, 848, L13
 Acernese F. et al., 2015, *Class. Quantum Gravity*, 32, 024001
 Amati L. et al., 2002, *A&A*, 390, 81
 Amati L. et al., 2018, *Adv. Space Res.*, 62, 191
 Andreoni I. et al., 2017, *Publ. Astron. Soc. Aust.*, 34, e069
 Antonelli L. A. et al., 2009, *A&A*, 507, L45
 Arcavi I., 2018, *ApJ*, 855, L23
 Arcavi I. et al., 2017, *Nature*, 551, 64
 Ascenzi S. et al., 2019, *MNRAS*, 486, 672
 Barbieri C., Salafia O. S., Perego A., Colpi M., Ghirlanda G., 2019, *A&A*, 625, A152
 Barnes J., Kasen D., Wu M.-R., Martínez-Pinedo G., 2016, *ApJ*, 829, 110
 Berger E., 2010, *ApJ*, 722, 1946
 Berger E. et al., 2007, *ApJ*, 664, 1000
 Berger E. et al., 2013a, *ApJ*, 765, 121
 Berger E., Fong W., Chornock R., 2013b, *ApJ*, 774, L23
 Bernardini M. G. et al., 2015, *MNRAS*, 446, 1129
 Blanton M. R., Roweis S., 2007, *AJ*, 133, 734
 Bloom J. S., Kulkarni S. R., Djorgovski S. G., 2002, *AJ*, 123, 1111
 Bloom J. S. et al., 2006, *ApJ*, 638, 354
 Brocato E. et al., 2018, *MNRAS*, 474, 411
 Bromberg O., Nakar E., Piran T., Sari R., 2012, *ApJ*, 749, 110
 Bulla M. et al., 2019, *Nat. Astron.*, 3, 99
 Cantiello M. et al., 2018, *ApJ*, 854, L31
 Cardelli J. A., Clayton G. C., Mathis J. S., 1989, *ApJ*, 345, 245
 Castro-Tirado A. J., Sanchez-Ramirez R., Lombardi G., Rivero M. A., 2015, *GCN Circ.*, 17758, 1
 Chan M. L., Messenger C., Heng I. S., Hendry M., 2018, *Phys. Rev. D*, 97, 123014
 Chornock R., Fong W., 2015, *GCN Circ.*, 17358, 1
 Chornock R., Lunnan R., Berger E., 2013, *GCN Circ.*, 15307, 1
 Chornock R., Fong W., Fox D. B., 2014, *GCN Circ.*, 17177, 1
 Chornock R. et al., 2017, *ApJ*, 848, L19
 Coulter D. A. et al., 2017, *Science*, 358, 1556
 Covino S. et al., 2017, *Nat. Astron.*, 1, 791
 Cowperthwaite P. S. et al., 2017, *ApJ*, 848, L17
 Cucchiara A., Levan A. J., 2016, *GCN Circ.*, 19565, 1
 D’Avanzo P. et al., 2009, *A&A*, 498, 711
 D’Avanzo P. et al., 2014, *MNRAS*, 442, 2342
 D’Avanzo P. et al., 2018, *A&A*, 613, L1
 D’Elia V., D’Avanzo P., Malesani D., di Fabrizio L., Tessicini G., 2013, *GCN Circ.*, 15310, 1
 de Ugarte Postigo A. et al., 2014, *A&A*, 563, A62
 Dichiaro S., Troja E., O’Connor B., Marshall F. E., Beniamini P., Cannizzo J. K., Lien A. Y., Sakamoto T., 2020, *MNRAS*, 492, 5011
 Drout M. R. et al., 2017, *Science*, 358, 1570
 Evans P. A. et al., 2017, *Science*, 358, 1565
 Fernández R., Metzger B. D., 2016, *Ann. Rev. Nucl. Part. Sci.*, 66, 23
 Fong W., Berger E., 2013, *ApJ*, 776, 18
 Fong W. et al., 2013, *ApJ*, 769, 56
 Fong W., Berger E., Margutti R., Zauderer B. A., 2015, *ApJ*, 815, 102
 Fong W. et al., 2016, *ApJ*, 833, 151
 Fong W. et al., 2017, *ApJ*, 848, L23
 Fox D. B. et al., 2005, *Nature*, 437, 845
 Gao H., Zhang B., Lü H.-J., Li Y., 2017, *ApJ*, 837, 50
 Gardner J. P. et al., 2006, *Space Sci. Rev.*, 123, 485
 Ghirlanda G. et al., 2019, *Science*, 363, 968
 Goldstein A. et al., 2017, *ApJ*, 848, L14
 Gompertz B. P. et al., 2018, *ApJ*, 860, 62
 Guillochon J., Parrent J., Kelley L. Z., Margutti R., 2017, *ApJ*, 835, 64
 Hallinan G. et al., 2017, *Science*, 358, 1579
 Hjorth J. et al., 2003, *Nature*, 423, 847
 Hjorth J. et al., 2017, *ApJ*, 848, L31
 Ivezić, Ž. et al., 2019, *ApJ*, 873, 111
 Izzo L., Cano Z., de Ugarte Postigo A., Kann D. A., Thoene C., Geier S., 2017, *GCN Circ.*, 21059, 1
 Jin Z.-P., Li X., Cano Z., Covino S., Fan Y.-Z., Wei D.-M., 2015, *ApJ*, 811, L22
 Jin Z.-P. et al., 2016, *Nat. Commun.*, 7, 12898
 Jin Z.-P. et al., 2018, *ApJ*, 857, 128
 Jin Z.-P., Covino S., Liao N.-H., Li X., D’Avanzo P., Fan Y.-Z., Wei D.-M., 2020, *Nat. Astron.*, 4, 77
 Kann D. A. et al., 2011, *ApJ*, 734, 96
 Kasen D., Fernández R., Metzger B. D., 2015, *MNRAS*, 450, 1777
 Kasen D., Metzger B., Barnes J., Quataert E., Ramirez-Ruiz E., 2017, *Nature*, 551, 80
 Kasliwal M. M. et al., 2017a, *Science*, 358, 1559
 Kasliwal M. M., Korobkin O., Lau R. M., Wollaeger R., Fryer C. L., 2017b, *ApJ*, 843, L34
 Kathirgamaraju A., Barniol Duran R., Giannios D., 2018, *MNRAS*, 473, L121
 Kathirgamaraju A., Tchekhovskoy A., Giannios D., Barniol Duran R., 2019, *MNRAS*, 484, L98
 Knust F. et al., 2017, *A&A*, 607, A84
 Kouveliotou C., Meegan C. A., Fishman G. J., Bhat N. P., Briggs M. S., Koshut T. M., Paciasas W. S., Pendleton G. N., 1993, *ApJ*, 413, L101
 Lamb G. P. et al., 2019, *ApJ*, 883, 48
 Levan A. J., Wiersema K., Tanvir N. R., Malesani D., Xu D., de Ugarte Postigo A., 2016, *GCN Circ.*, 19846, 1
 LIGO Scientific Collaboration, 2015, *Class. Quantum Gravity*, 32, 074001
 Li L.-X., Paczyński B., 1998, *ApJ*, 507, L59
 Lyman J. D. et al., 2018, *Nat. Astron.*, 2, 751
 Maiorano E., Amati L., Rossi A., Stratta G., Palazzi E., Nicastro L., 2018, *Mem. Soc. Astron. Ital.*, 89, 181

- Malesani D., D'Avanzo P., D'Elia V., Vergani S. D., Andreuzzi G., Garcia A., Escudero G., Bonomo A., 2014, *GCN Circ.*, 17170, 1
- Malesani D. et al., 2015, *GCN Circ.*, 17755, 1
- Mandel I., 2018, *ApJ*, 853, L12
- Mangano V. et al., 2007, *A&A*, 470, 105
- Margutti R. et al., 2012, *ApJ*, 756, 63
- Margutti R. et al., 2018, *ApJ*, 856, L18
- Metzger B. D., 2017, *Living Rev. Relativ.*, 20, 3
- Metzger B. D., Piro A. L., 2014, *MNRAS*, 439, 3916
- Metzger B. D. et al., 2010, *MNRAS*, 406, 2650
- Metzger B. D., Thompson T. A., Quataert E., 2018, *ApJ*, 856, 101
- Mooley K. P. et al., 2018a, *Nature*, 554, 207
- Mooley K. P. et al., 2018b, *Nature*, 561, 355
- Nicuesa Guelbenzu A. et al., 2011, *A&A*, 531, L6
- Nicuesa Guelbenzu A. et al., 2012, *A&A*, 548, A101
- Perego A., Radice D., Bernuzzi S., 2017, *ApJ*, 850, L37
- Perley D. A., 2015, *GCN Circ.*, 17744, 1
- Perley D. A., Cenko S. B., 2015, *GCN Circ.*, 17312, 1
- Perley D. A. et al., 2009, *ApJ*, 696, 1871
- Perley D. A., Modjaz M., Morgan A. N., Cenko S. B., Bloom J. S., Butler N. R., Filippenko A. V., Miller A. A., 2012, *ApJ*, 758, 122
- Pian E. et al., 2017, *Nature*, 551, 67
- Piro L. et al., 2019, *MNRAS*, 483, 1912
- Planck Collaboration XIII, 2016, *A&A*, 594, A13
- Price P. A., Berger E., Fox D. B., 2006, *GCN Circ.*, 5275, 1
- Radice D., Perego A., Hotokezaka K., Fromm S. A., Bernuzzi S., Roberts L. F., 2018, *ApJ*, 869, 130
- Rossi A., Stratta G., Maiorano E., Amati L., Nicastro L., Palazzi E., 2018a, *Mem. Soc. Astron. Ital.*, 89, 254
- Rossi A. et al., 2018b, *GCN Circ.*, 22763, 1
- Sakamoto T. et al., 2013, *ApJ*, 766, 41
- Salafia O. S., Ghirlanda G., Ascenzi S., Ghisellini G., 2019, *A&A*, 628, A18
- Sari R., Piran T., Narayan R., 1998, *ApJ*, 497, L17
- Sari R., Piran T., Halpern J. P., 1999, *ApJ*, 519, L17
- Sathyaprakash B. et al., 2012, *Class. Quantum Gravity*, 29, 124013
- Savchenko V. et al., 2017, *ApJ*, 848, L15
- Schlaflly E. F., Finkbeiner D. P., 2011, *ApJ*, 737, 103
- Selsing J. et al., 2018, *A&A*, 616, A48
- Selsing J. et al., 2019, *A&A*, 623, A92
- Siegel D. M., Ciolfi R., 2016a, *ApJ*, 819, 14
- Siegel D. M., Ciolfi R., 2016b, *ApJ*, 819, 15
- Smartt S. J. et al., 2017, *Nature*, 551, 75
- Spyromilio J., Comerón F., D'Odorico S., Kissler-Patig M., Gilmozzi R., 2008, *Messenger*, 133, 2
- Stratta G. et al., 2007, *A&A*, 474, 827
- Stratta G. et al., 2018a, *Adv. Space Res.*, 62, 662
- Stratta G., Dainotti M. G., Dall'Osso S., Hernandez X., De Cesare G., 2018b, *ApJ*, 869, 155
- Tanaka M. et al., 2018, *ApJ*, 852, 109
- Tanvir N. R. et al., 2010, *GCN Circ.*, 11123, 1
- Tanvir N. R., Levan A. J., Fruchter A. S., Hjorth J., Hounsell R. A., Wiersema K., Tunnicliffe R. L., 2013, *Nature*, 500, 547
- Tanvir N. R. et al., 2015, *GCN Circ.*, 18100, 1
- Tanvir N. R. et al., 2017, *ApJ*, 848, L27
- Troja E. et al., 2016, *ApJ*, 827, 102
- Troja E. et al., 2017, *Nature*, 551, 71
- Troja E. et al., 2018a, *Nat. Commun.*, 9, 4089
- Troja E. et al., 2018b, *MNRAS*, 478, L18
- Troja E. et al., 2019, *MNRAS*, 489, 2104
- Varela K., Knust F., Greiner J., 2015, *GCN Circ.*, 17732, 1
- Villar V. A. et al., 2017, *ApJ*, 851, L21
- Yang B. et al., 2015, *Nat. Commun.*, 6, 7323
- Yaron O., Gal-Yam A., 2012, *PASP*, 124, 668
- Yonetoku D., Murakami T., Nakamura T., Yamazaki R., Inoue A. K., Ioka K., 2004, *ApJ*, 609, 935
- Yu Y.-W., Zhang B., Gao H., 2013, *ApJ*, 776, L40
- Zhang B., Mészáros P., 2001, *ApJ*, 552, L35
- Zhang B., Mészáros P., 2004, *Int. J. Mod. Phys. A*, 19, 2385
- Zhang B., Fan Y. Z., Dyks J., Kobayashi S., Mészáros P., Burrows D. N., Nousek J. A., Gehrels N., 2006, *ApJ*, 642, 354

SUPPORTING INFORMATION

Supplementary data are available at *MNRAS* online.

Figure A3. Short GRB optical counterparts for which the luminosity light curves are above the AT2017gfo luminosity in any filter.

Figure A4. Same as Fig. A1 but for three examples of short GRB optical counterparts for which the luminosity light curves do not cover the AT2017gfo sampled temporal window and no direct (i.e., with no extrapolation) luminosity comparison could be performed.

Table A1. Table with GRB and AT2017gfo luminosity ratios.

Table A2. Short GRBs with known redshift in addition to Fong et al. (2015).

Table A3. Rest-frame light curves of AT2017gfo.

Please note: Oxford University Press is not responsible for the content or functionality of any supporting materials supplied by the authors. Any queries (other than missing material) should be directed to the corresponding author for the article.

APPENDIX A: ADDITIONAL MATERIAL

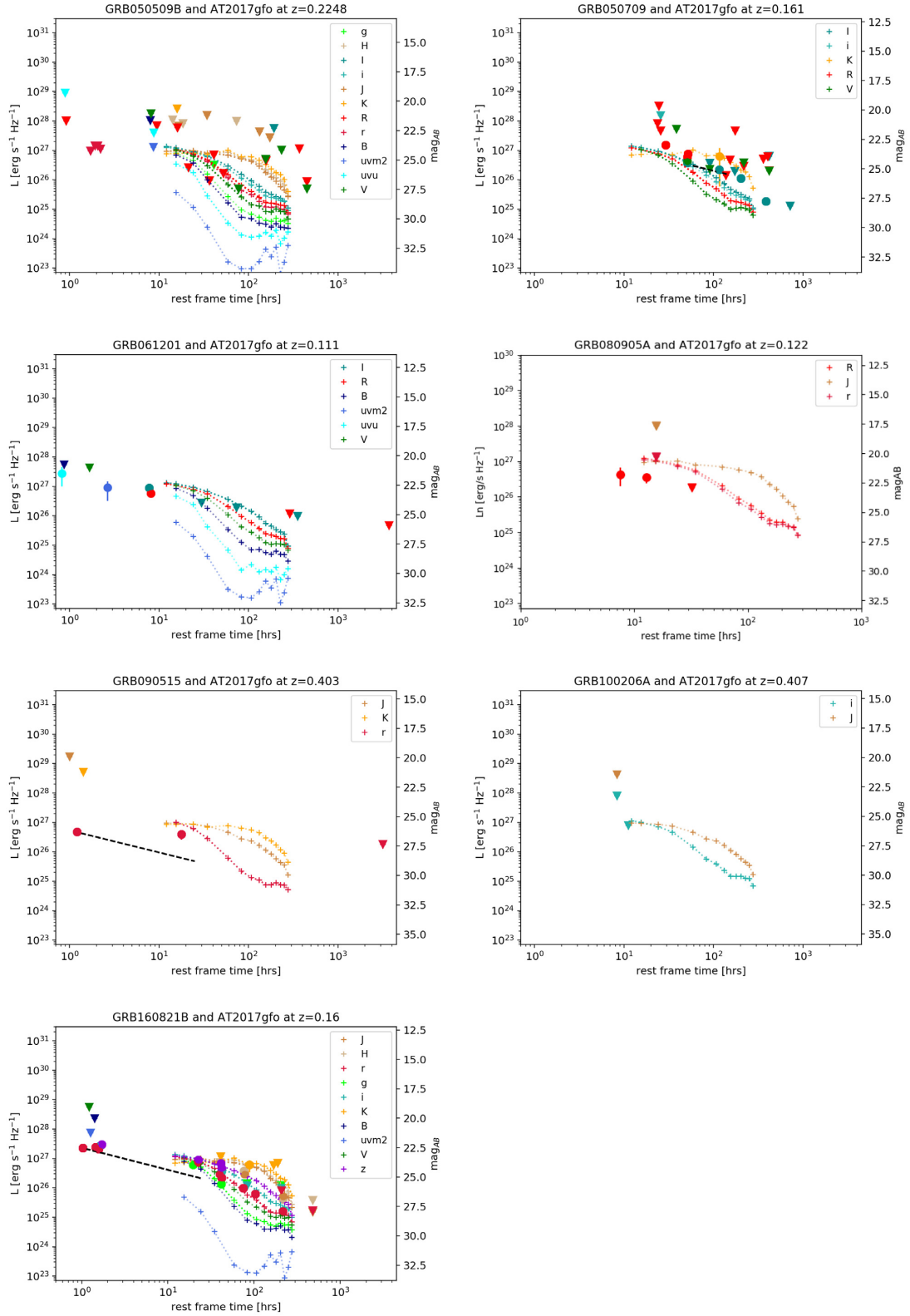


Figure A1. Short GRBs for which the optical counterpart luminosity (circles mark the detections and triangles the upper limits) are fainter than AT2017gfo luminosity (dotted lines with crosses) in at least one effective rest-frame filter (see Section 3.2). Note that GRB 050709, GRB 090515, and GRB 160821B show evidence of a temporal decay index lower than the shallowest index predicted by the fireball model (i.e. $\alpha < 0.75$, see Section 4.2, black dashed line).

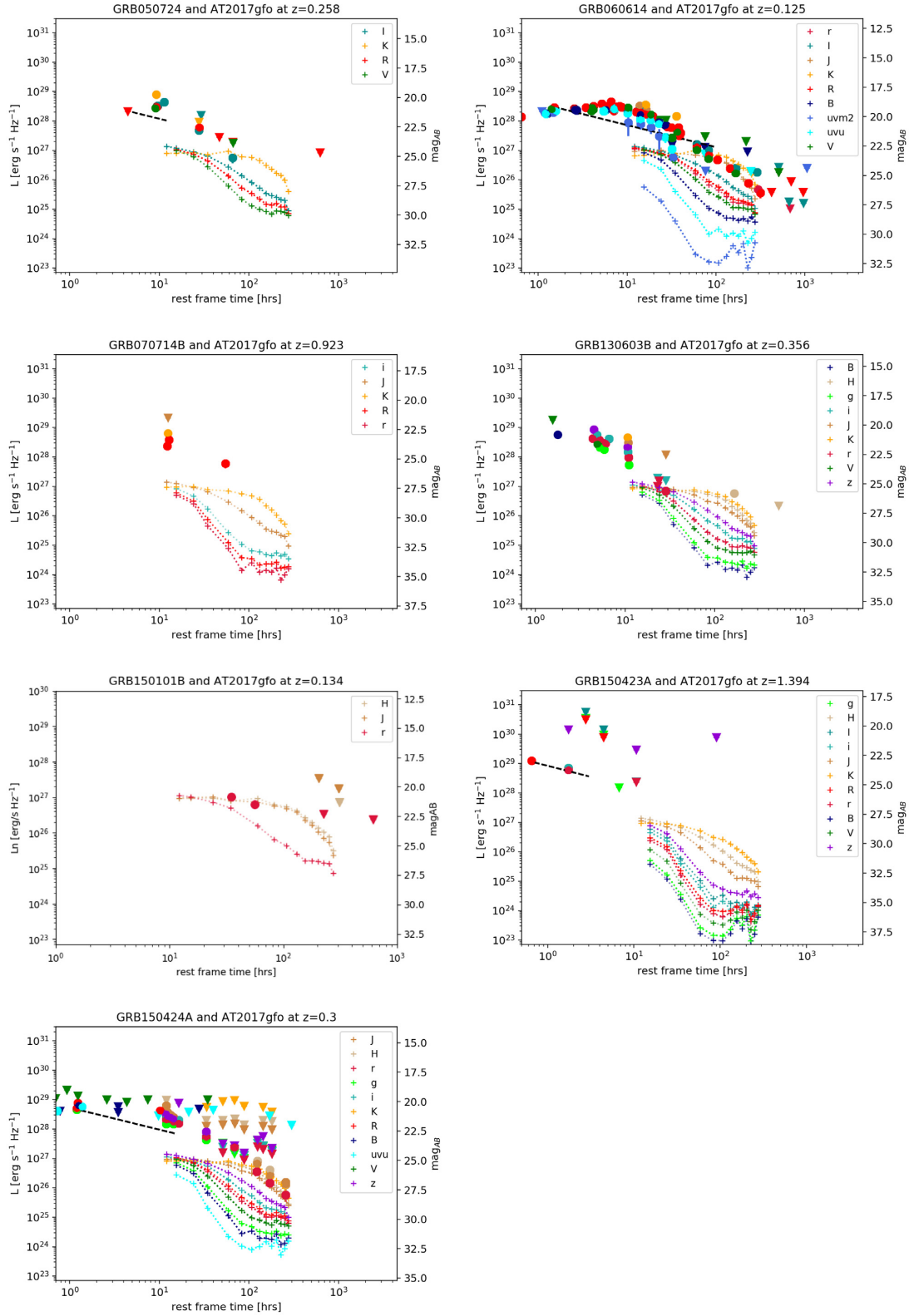


Figure A2. Same as Fig. A1 but for GRB optical counterparts for which the luminosity light curves are above the AT2017gfo luminosity in any filter and for which we found evidence of an anomalous shallow decay. If this feature is due to an emerging KN emission, from these short GRBs we can infer the upper range of possible N luminosity values (i.e. not just upper limits). We include here also the light curves of GRBs 070714B, 130603B, and 150101B for which a KN is claimed in the literature.

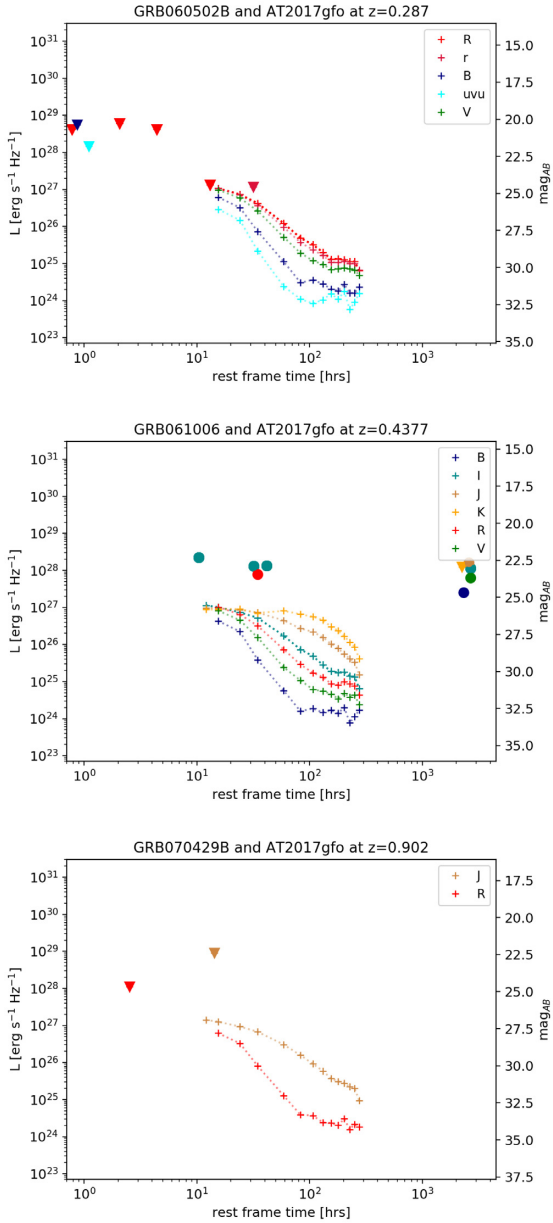


Figure A3. Short GRB optical counterparts for which the luminosity light curves are above the AT2017gfo luminosity in any filter. Circles mark the detections and triangles mark the upper limits, AT2017gfo luminosity is indicated with dotted lines with crosses. The plots of the whole sample are available online.

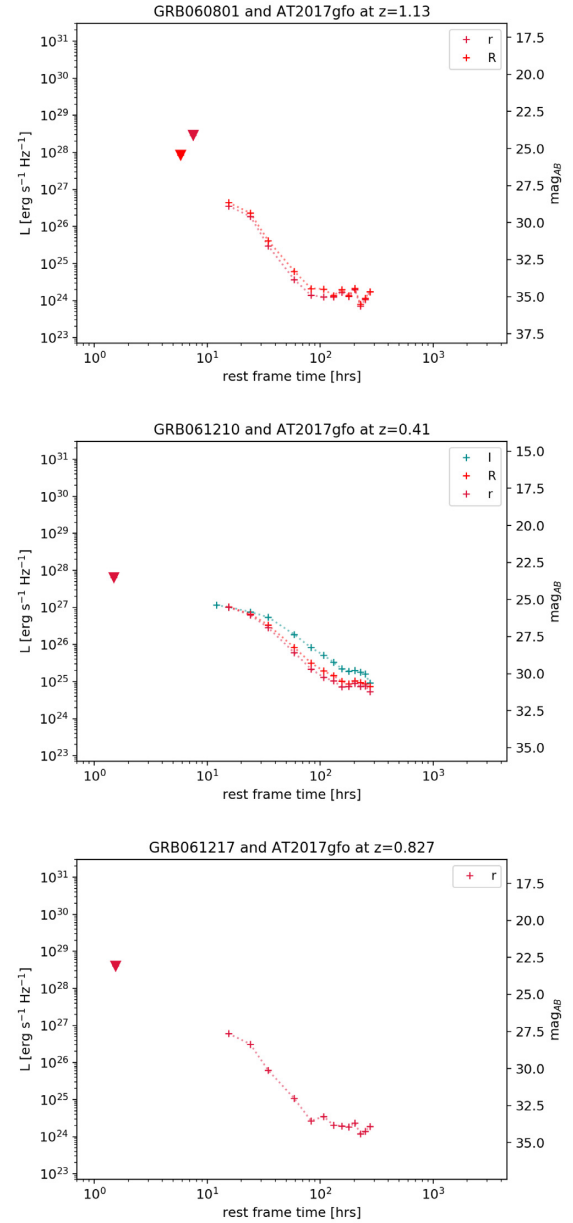


Figure A4. Same as Fig. A1 but for three examples of short GRB optical counterparts for which the luminosity light curves do not cover the AT2017gfo sampled temporal window and no direct (i.e. with no extrapolation) luminosity comparison could be performed. The plots of the whole sample are available online.

Table A1. Table with GRB and AT2017gfo luminosity ratios. The full table is available online.

GRB	Time (h)	Band eff.	L_{GRB} (10^{26} erg s $^{-1}$ Hz $^{-1}$)	L_{KN} (10^{26} erg s $^{-1}$ Hz $^{-1}$)	$L_{\text{GRB}}/L_{\text{KN}}$	z	λ_{rest} (nm)	λ_{obs} (nm)
050509B	40.9	<i>g</i>	<3.21	1.24	<2.59	0.225	391.7	479.8
050509B	77.1	<i>V</i>	<0.50	0.36	<1.38	0.225	454.9	557.1
050509B	155.6	<i>V</i>	<5.01	0.08	<59.43	0.225	454.9	557.1
050509B	233.0	<i>V</i>	<10.50	0.08	<123.82	0.225	454.9	557.1
050509B	16.1	<i>R</i>	<60.60	10.50	<5.77	0.225	523.5	641.2

Table A2. Short GRBs with known redshift in addition to Fong et al. (2015). The full table is available online.

GRB	ΔT (h)	Telescope/Instr	Filter	Mag	Flux density (μJy)	Gal. Ext. A_V	Refs
050509B	0.37175	1.3 m PAIRITEL	<i>J</i>	>19.30	<71.79	0.05	Bloom et al. (2006)
	0.37175	1.3 m PAIRITEL	<i>H</i>	>19.50	<59.41		
	0.37175	1.3 m PAIRITEL	<i>K_s</i>	>18.95	<98.36		
	0.55656	3.5 m WIYN OPTIC CCD	<i>i</i>	>20.95	<15.97		
	0.63008	3.5 m WIYN OPTIC CCD	<i>i</i>	>22.05	<5.80		

Table A3. Rest-frame light curves of AT2017gfo. The full table is available online.

Time (d)	Luminosity (erg s $^{-1}$ Hz $^{-1}$)	M_{abs} AB	Filter	Time (d)	Luminosity (erg s $^{-1}$ Hz $^{-1}$)	M_{abs} AB	Filter
0.50	–	–	<i>U</i>	0.50	1.29E+27	–16.16	<i>r</i>
0.64	7.18E+26	–15.52	<i>U</i>	0.64	1.15E+27	–16.03	<i>r</i>
0.99	3.81E+26	–14.83	<i>U</i>	0.99	8.50E+26	–15.70	<i>r</i>
1.49	1.02E+26	–13.40	<i>U</i>	1.49	6.22E+26	–15.36	<i>r</i>
2.43	1.65E+25	–11.42	<i>U</i>	2.43	2.43E+26	–14.35	<i>r</i>
3.47	5.35E+24	–10.20	<i>U</i>	3.47	1.18E+26	–13.56	<i>r</i>
4.41	4.51E+24	–10.01	<i>U</i>	4.41	6.90E+25	–12.98	<i>r</i>
5.45	3.18E+24	–9.64	<i>U</i>	5.45	4.64E+25	–12.54	<i>r</i>
6.44	2.99E+24	–9.57	<i>U</i>	6.44	3.03E+25	–12.08	<i>r</i>
7.43	3.21E+24	–9.65	<i>U</i>	7.43	2.65E+25	–11.94	<i>r</i>

This paper has been typeset from a \LaTeX file prepared by the author.